INTERNATIONAL ATOMIC ENERGY AGENCY
UNITED NATIONS EDUCATIONAL, SCIENTIFIC AND CULTURAL ORGANIZATION

INTERNATIONAL CENTRE FOR THEORETICAL PHYSICS
34100 TRIESTE (ITALY) - P.O.B. 586 - MIRAMARE - STRADA COSTIERA 11 - TELEPHONE: 2240-1
CABLE: CENTRATOM - TELEX 460392 - I

SMR/459-7

SPRING COLLEGE IN CONDENSED MATTER
ON
'PHYSICS OF LOW-DIMENSIONAL STRUCTURES'
(23 April - 15 June 1990)

NOVEL SEMICONDUCTOR MATERIALS AND STRUCTURES

R.A. STRADLING
Imperial College of Science, Technology and Medicine
The Blackett Laboratory
Department of Physics
Prince Consort Road
London SW7 2AZ
United Kingdom

NOVEL SEMICONDUCTOR MATERIALS AND STRUCTURES

R.A. Stradling,

London University Interdisciplinary Research Centre in Semiconductor Materials and the Blackett Laboratory, Imperial College, London SW7 2BZ, UK.

Abstract

The development of new epitaxial techniques has given rise to a variety of new material combinations. Pseudomorphic combinations where the partners have lattice constants which differ by more than 1% are currently being extensively studied. The built-in strain can alter the symmetry and magnitudes of the band gaps concerned. Interesting examples of systems currently being investigated are strained layer superlattices based on $Si/Si_{1-x}Ge_x$, GaAs/InAs and $InSb/InSb_{1-x}As_x$.

The growth and properties of narrow gap semiconductor systems are reviewed together with their use as components for strained layer structures. The materials discussed are InSb, InAs, the alloys of these two compounds and alpha tin. The alloy system $InAs_xSb_{1-x}$ is prone to metallurgical problems such as ordering and phase separation in the mid alloy range but high mobility samples have been grown. Other alloy systems, e.g. $Al_{1-x}In_xAs$, are currently of great interest and are also prone to similar problems.

The electrical and optical properties of mismatched systems are discussed both as strained layer superlattices and in relaxed structures. One of the most interesting and surprising results concerns the observation of a strong Shubnikov-de Haas effect and mobilities close to the bulk value in ultrathin films of weakly doped InSb grown on mismatched GaAs substrates. This result demonstrates that the dislocations found in the interface region are only weakly charged and therefore do not scatter the carriers significantly.

The strain associated with the small but significant mismatch between α-Sn and InSb stabilises the alpha phase up to 100°C and opens up an energy gap of 0.2eV. The first observation of the Shubnikov-de Haas effect with this heterostructure system demonstrates the presence of a high density two-dimensional electron gas at the interface. The carrier density is too high to arise solely from the band offsets. A complicated cyclotron resonance spectrum is observed.

Spike-doped and n-i-p-i structures are studied in InSb and InAs. Minimal dopant diffusion is found and highly non-linear optical absorption and a striking Quantum Hall Effect are also observed. The possibilities for devices based on intersubband transitions in spike-doped and quantum well structures are also discussed.

1. Introduction

The most developed low-dimensional semiconductor structures, both for fundamental studies and in device applications, are those based on abrupt heterostructures between GaAs and AlGaAs. This system depends for its success on the near-perfect match between the binary components, GaAs and AlAs. However, neither silicon nor GaAs has a band-gap suitable for long wavelength optical sources, signal processing devices or detectors. Consequently developments in optoelectronics have produced demands for new semiconductor materials and device concepts. A variety of new materials systems are now emerging where the components are deliberately chosen to be grossly mismatched. In many cases mismatch epitaxy is used deliberately to change the symmetry of the bands and to modify the band gaps (eg. $Ga_{1-x}In_xAs/GaAs$ and $Si/Si_{1-x}Ge_x$ strained layer superlattices). In the case of $InAs_{1-x}Sb_x$ strained layer quantum wells the long wavelength barrier of 10μm can be breached although both components of the heterostructures have band gaps corresponding to shorter wavelengths. However, as will be discussed in this paper, there are severe metallurgical problems in the mid-alloy range with this system.

The strain can also be used to increase the phase stability of one component as for alpha-tin grown on InSb or CdTe. This system shows a very pronounced two-dimensional electron gas at the interface of a single heterostructures. Another example of a novel materials system is the binary compound InBi.

There is a need with the new materials systems to integrate structures onto well established materials such as silicon or GaAs. With some systems (eg. InSb or InAs on GaAs or GaAs on Si) the mismatch is too great to permit the growth of thick epitaxial layers although it is desirable for other reasons to create structures of these combinations. In these cases the layers are allowed to relax and a high density of misfit and threading dislocations form at the interface. A surprising result is that strong Shubnikov-de Haas oscillations and mobilities close to the bulk value can be observed in lightly doped ultrathin sample of InSb grown on GaAs substrates. This result suggest that the dislocations (predominantly edge in character) are only weakly charged and do not therefore degrade the majority carrier properties significantly.

Spike or delta doping where the dopants are deposited on a single atomic plane gives rise to the possibility of building in electric fields as high as 10^6V/cm into semiconductor structures. The fabrication of n-i-p-i structures can give rise to large reductions in band-gap, long lifetimes and big optical nonlinearities. Quantum transport measurements can be used to study dopant diffusion and an interesting Quantum Hall Effect is seen in the limit of extreme disorder.

Another alternative to narrow gap semiconductors for devices operating in the long wavelength regime is the use of intersubband transitions in quantum wells or doping structures.

A novel development in strained layer systems concerns the incorporation of single monolayers of grossly mismatched materials in a matrix of another material (eg. single layers of InAs or GaSb in GaAs - good quality samples of both systems have been demonstrated). It becomes a semantic question as to whether this should be considered as delta isoelectronic doping or an ultrathin strained layer system.

2. The MBE Growth of Narrow-Gap III-V Materials

2.1 The Growth of InAs and InSb

High purity InSb and InAs layers have been grown both homoepitaxially and also heteroepitaxially on GaAs [1,2]. In both cases the background donor contamination level was found to be comparable to that in MBE GaAs.

2.1.1. The Characterisation of InAs

The value of farinfrared measurements in characterising semiconductor samples (see Appendix A) was strikingly demonstrated for the MBE layers of InAs. When laser magneto-optical studies were performed, it was clear that there were two types of carrier present in the layers (see figure one). The broad line seen at high fields can be identified as arising from cyclotron resonance from a two-dimensional electron gas from its shift to higher fields on rotating the magnetic field away from the perpendicular to the surface. The sharper lines to lower field are unaffected on tilting the field and therefore come from carriers located in the bulk of the film. In order of decreasing field the sharp lines are firstly the cyclotron resonance from the bulk carriers, then the $1s-2p_+$ line from the shallow donors and then subsequently the $1s-3d_{+2}$ and higher order donor lines. No evidence for dislocation scattering was found as the cyclotron resonance line width was independent of the film thickness. The two dimensional electron gas responsible for most of the oscillator strength of the transitions shown in figure one is thought to arise from a surface accumulation layer. The surface accumulation is thought to arise from amphoteric native defects in the surface region. Alone amongst III-V materials the presence of these defects in InAs presents a major problem for device applications as their energy levels lie outside the forbidden gap and consequently pin the Fermi energy in the conduction band. As a result the surface in any lateral or mesa structure will always provide a shorting conduction path unless the native defects are passivated.

The idea of the amphoteric native defect has been developed by Spicer and coworkers [3] and by Walukiewicz [4]. Almost identical energy levels are found at metal-semiconductor and air-semiconductor interfaces and also in the bulk on particle irradiation. These defects can also limit the doping activity of substitutional impurities and the ability to dope InAs heavily n-type compared with InSb or GaAs (see following paragraphs) appears to be related to the location of the levels from the native defect approximately 150meV into the conduction band (figure 2). Schottky barrier heights measured for metal-semiconductor junctions are to a considerable extent independent of the metal concerned because of the existence of the native defect levels. Monch [5] has shown empirically that Schottky barrier heights do not depend simply on the magnitude of the direct energy gap but a remarkably linear relationship is obtained if the barrier heights are plotted against the values of the indirect gap for a variety of semiconductors. It would seem therefore that the reason that InAs is so prone to surface accumulation is that the indirect band gap is so much greater than the direct which results in the native defect levels lying in the lower conduction band.

Electrical measurements with these epitaxial InAs films provide a good example of how Hall measurements can be misinterpreted. The conducting skin formed by the electron accumulation layer severely affects the measurements, particularly with thin films, leading to grossly misleading values of mobility and carrier concentration if interpreted on a single carrier model.

As can be seen in figure three, the mobility derived from the product ($R\sigma$) decreases rapidly with decreasing film thickness. A similar variation had been noted by another group and attributed to the onset of scattering by misfit dislocations located close to the interface. The magneto-optical experiments shown in figure one demonstrated that the samples consisted of two different conducting regions, ie. a high mobility region in the centre of the film with sharp donor states separated from a low mobility two-dimensional electron gas (2DEG) caused by surface states. The mobilities in the two regions could be estimated from the magneto-optical line widths and the number of carriers in each of the two regions could be determined; in the one case from the Shubnikov-de Haas effect (appendix B) observed by the 2DEG formed by the surface accumulation layer and, for the bulk electrons, from the absolute value of the absorption coefficient found from the intensity of the cyclotron resonance line.

The boundary condition for the Hall current generated with a magnetic field perpendicular to the film is identical to that for two carrier conduction in a homogeneous medium (ie the net current has to be zero). Hence equations (B2) and (B4), modified by replacing the volume carrier densities by the concentrations per unit area, can be used to model the field dependence of the Hall coefficient and the magnetoresistance, and also the thickness dependence of the apparent carrier concentration deduced from a simplistic interpretation of the Hall coefficient (figure 3). It can

be seen that the two carrier modelling predicts the observed drop in Hall mobility as the sample thickness is decreased without the need to include dislocation scattering.

In addition it should be noted that, because of the very high mobility for the electrons in the bulk of the film, the magnetic field has to be reduced to the extremely low value of 0.01T before the low field limit applies and the Hall coefficient is independent of field. The absolute values for the magneto-resistance are predicted accurately, the values for the apparent mobility and n less so. The reason for this difference between experiment and model probably lies in the existence of a third conducting region close to the InAs/GaAs interface rather than in a significant error in the fitting parameters.

It should also be noted that, despite the carrier concentrations in both the surface and bulk regions being independent of temperature between 290 and 77K, the Hall coefficient increased by more than a factor of two in this temperature range. This temperature dependence arises because the mobility in the bulk region is increasing rapidly with decreasing temperature whereas that in the low mobility surface skin is independent of temperature. A freeze-out of electrons onto impurity sites would be deduced if a single carrier model were assumed although in fact no such deactivation was taking place.

2.1.2 The Growth and doping of InSb

RHEED oscillations were observed for the first time with InSb [6]. They are now used routinely for determining the growth rates and to set up the starting conditions. The optimum flux ratio for maximum RHEED oscillation amplitude was much lower than the ratios commonly employed.

The doping of InSb and InAs by silicon and beryllium has been explored. In the case of bulk InSb silicon is known to be strongly amphoteric with p-type activity and a compensation ratio of 0.3 [7]. In contrast silicon acts as a donor in MBE material and, provided that the growth temperature is kept below 350°C, virtually 100% donor activation is achieved up to concentrations of 5 x 10^{18} cm^{-3}. In InAs silicon is incorporated as a donor up to very high concentrations and levels of about 10^{20} cm^{-3} are achievable. With both InSb and InAs we have shown that Be can produce hole levels up to $5x10^{19}$ cm^{-3}. The higher silicon donor concentrations achievable with InAs compared with InSb or GaAs is in accord with the concept of the native amphoteric defect and its role in determining the site occupancy of the group IV dopants. Alone amongst the III-V compounds the native defect level is resonant with the conduction band in InAs. With InAs therefore greater concentrations of silicon can be incorporated on the group III site without the Fermi energy rising too far above the energy of the native defect level. High levels of doping with both silicon and tin have also been reported for $In_{0.53}Ga_{0.47}As$ [8]. Peak levels of $1.5x10^{19}$ and $4x10^{19}$ cm^{-3} were found with silicon and tin respectively, ie. the maximum concentrations achievable were intermediate between those for GaAs and InAs.

The MOCVD doping of InSb has also been investigated in detail [9]. Donor concentrations in excess of 10^{19} cm^{-3} are achievable using tellurium. However this element in common with its use in MBE [10] was found to suffer from a severe memory effect which produced a background contamination level of the order of $5x10^{16}$ cm^{-3} in samples grown subsequently in a reactor which had been used for tellurium doping. Attempts to introduce donors using silane and hydrogen selenide as the dopant gases resulted in poor surface morphologies and a reduction by up to an order of magnitude in the growth rate. This behaviour is indicative of an interaction between the dopant gas and the metal-organics in the vapour phase.

The ability to control the dopants in MBE growth of these materials has allowed us to use atomic plane doping to produce delta spike-doped single well structures, and delta n-i-n-i and n-i-p-i structures (see section 5).

2.2 The Growth of III-V Alloys

The alloy system $InSb_{1-x}As_x$ is of considerable interest as strained-layer superlattices with band-gaps corresponding to wavelengths longer than 10μm have been grown with this system [11]. In our work the use of in-situ RHEED has enabled the accurate calibration of the Group V fluxes, thus permitting the production of alloys within 2% of the expected composition. As a result of the RHEED measurements we should now be able to reproducibly grow superlattices of $InAs_xSb_{1-x}/InAs_{1-y}Sb_y$ over a wide range of thickness or composition. Depending upon the growth temperature, the 77K Hall mobility of these alloys can drop by as much as three orders of magnitude in mid-range compared with the mobilities measured for the binary compounds (figure four) . This is a surprising result because the level of contamination in the growth system is very low as demonstrated by the high quality of both the InAs and InSb samples produced. It is believed that this drop of mobility in the MBE alloys arises from structural problems. High on the list of possible mechanisms for the drop in the mobility in the alloys are the ordering effects which have recently been observed [12] in transmission electron diffraction which include localised ordering, the formation of clusters and even phase separation in the mid-alloy range (see figure five for the remarkable platelet structure associated with the phase separation which occurs when the alloys are grown at relatively low temperatures. This type of electrical inhomogeneity on the scale of the electron mean free path will severely distort the current flow in the sample and give rise to highly misleading Hall measurements. The dangers of

a simplistic interpretation of mobility in an inhomogeneous medium were amply demonstrated in respect of the thin heteroepitaxial samples discussed in 3.2. We are now carrying out a careful comparison of the electrical, optical and structural properties of the alloys in order to establish the correlation with alloy ordering clustering and phase separation.

Excellent results for both surface morphology and mobility have been obtained for MBE growth of the alloy system using a dimer source for the As and a tetramer source for the Sb [13]. A mobility of 40,000cm^2/Vs was obtained with a sample of 3μm thickness containing 34% InAs. With these samples a graded buffer layer was used and it is not yet clear how much of the improvement in material quality was due to the different surface chemistry involved in mixing dimer and tetramer sources.

Another alloy system where ordering and clustering can be a problem is $Al_{1-x}In_xAs$ as there are large differences in the In and Al related bond energies. The interest in this system is that it is lattice matched to InP at a composition x=0.52 and (GaIn)As/(AlInAs) HEMTs show superior microwave performance to (GaInAs/InP) structures, probably because of the larger conduction band offsets. This large offset for (GaIn)As/(AlIn)As has enabled intersubband multiple-quantum-well detectors operating at wavelengths as short as 5μm to be fabricated [14].

Another interesting narrow gap combination is InAs/AlSb. These two compounds are closely lattice matched and have a conduction band offset which is thought to be in the range 1.35 to 1.9eV, ie. even larger than that for the the (GaIn)As/(AlIn)As system. Excellent electrical properties including quantum Hall measurements have been reported for this system [15,16]. However, both the anion and cation change across the interface and the electrical quality depends strongly on the sequence in which the quantum well interfaces are grown because of the possibility of formation of antisite donors at the interface. High mobilities are only seen when the bottom interface is InSb-like.

In the search for materials having optimal properties, GaSb/AlSb, GaSb/InAs and $InSb/In_{1-x}Al_xSb$ are being investigated for long wavelength applications and the quaternary systems (GaIn)(AsP) and (GaIn)(AsSb) for applications in the 1.3 to 1.6μm wavelength band.

Alternative III-V systems which are currently being investigated for the mid-infrared wavelength range are the strained layer systems discussed in section 3.3, the n-i-p-i structures discussed in section five and also $InSb_{1-x}Bi_x$ [17] and $InAs_{1-x}Bi_x$.With the latter system the band gap of InAs was reduced by 25% on introducing 2% Bi [18] An even more exotic possibility for this wavelength region is the alpha tin/germanium alloy system which can be combined with InSb or CdTe as discussed in section four. With both the SnGe alloy system and the narrow gap III-Vs alloyed with Bi, the alloys are metastable but can be grown by thin-layer epitaxial techniques.

3 Mismatch epitaxy

Mismatch epitaxy is now widely employed to fabricate heterostructures where the lattice constants of the two component materials differ by ≥ ½%. In strained layer superlattices (SLS) the epitaxial layers of the two components are thinner than the critical thickness for the formation of misfit dislocations with the result that the layers remain in registry. In this case the resulting strain is deliberately used to modify the band structure of the system. With SLS the materials are generally chosen so that the mismatch is relatively small so that quite thick layers can be grown without dislocations forming. In many other cases, it may desirable to combine materials with very different electrical or optical properties despite the large mismatch precluding the pseudomorphic growth of more than a few monolayer (i.e. when the mismatch exceeds a few percent). Examples of such materials combinations are InSb or InAs on GaAs where GaAs substrates are chosen because of their cheapness and their electrical insulating properties; and GaAs on Si where the aim is to integrate optoelectronic and microelectronic devices on the same chip. With these systems the strain is relieved in the interface region by the formation of a high density of misfit dislocations and relatively thick layers may then be grown with reasonable electrical and optical quality with the epitaxial material in the almost completely relaxed and unstrained state.

3.1 Electrical measurements in relaxed films of InSb and InAs

If the components are grossly mismatched and epitaxial films are grown at thicknesses much greater than the critical thickness above which the lowest energy state is the layer having its natural lattice spacing, a very high density of misfit dislocations ($10^{11}cm^{-2}$) will be found close to the interface and the film is almost completely relaxed. The dislocation density falls below 10^7cm^{-2} after growth has continued for a few microns. There is an almost universal belief that a high density of dislocations will dramatically degrade the electrical properties of semiconductors and there are many reported cases of materials systems where the Hall mobility falls rapidly as the thickness of the epitaxial layers is decreased. The dependence of the Hall effect, conductivity and magnetoresistance on temperature and film thickness has been investigated for a series of thin layers of InSb grown by Molecular Beam Epitaxy (MBE) on GaAs substrates where the dislocation density is high throughout the films (the lattice mismatch is 14% for this system). GaAs is a popular substrate for narrow gap semiconductors such as InSb and InAs as it provides good isolation for electrical measurements. Even with thick InSb films grown on mismatched substrates, Hall measurements have generally indicated electron concentrations substantially higher and mobilities up to several orders of magnitude lower than those found with homoepitaxial material grown in the same reactor.

In the present work early stages of growth were monitored by RHEED and the layers grown were studied subsequently by TEM [19]. Multiply connected islands were found until the thickness reached 0.1μm. Beyond this thickness the films were flat and parallel sided.

The average carrier concentration (n) determined by the Hall effect increased rapidly with decreasing thickness and the mobility (μ) fell at a slightly greater rate (see fig six). The magnetic field employed for the Hall measurements was below 0.05T to ensure that a low field analysis could be applied. No conductivity could be measured at thicknesses below 0.08μm. Also included in the figure are 77K mobility results for magnetron sputtered samples of lower purity than the MBE samples [20].

The observation of a strong thickness dependence of the measured electrical parameters by itself suggests the presence of layered conductivity. This in turn implies that the measurements require reinterpretation in terms of parallel conductance effects. Simple mathematical models have been developed assuming single-carrier layered n-type conductivity which show the correct functional form of the dependence of mobility and carrier concentration on thickness. However the magnetoresistance and field dependence of the Hall constant (r) predicted by these models were always about two orders of magnitude smaller than those observed experimentally whatever the analytic function chosen to describe the dependence of carrier concentration and mobility on thickness. Thus, although at first sight it would seem that dislocations are responsible for the apparent degradation of the electrical properties, the strong field dependence of r and the large magnetoresistance cannot be explained on this picture.

Furthermore measurements with samples backdoped with silicon show that the bulk electrical parameters can be recovered even with very thin samples at modest doping levels. Two structures were studied. The first consisted of a slab-doped region 1000A thick with a carrier concentration of $2x10^{17}cm^{-3}$ grown starting at the interface in an InSb film of total thickness 1.2μm. The mobility at 77K of 15,000 cm^2/Vs was within a factor of two of the normal ionised impurity mobility for bulk samples at the doping concentration concerned. The doping concentration coincidentally was close to the value measured with thin samples of thickness 0.1μm. Yet the mobility measured with the thin undoped samples (100 cm^2/Vs at 1500A and 20 cm^2/Vs at 800A) was more than three orders of magnitude lower than that found with the thicker sample containing the doping slab. The second doped structure consisted of a very thin film of total thickness of 0.15 μm grown on GaAs at 330°C with the last 0.05 μm doped with silicon to a concentration of $2x10^{17}cm^{-3}$. The carrier concentration measured in a weak field Hall experiment was identical to the doping level and the mobility of 29,000 cm^2/Vs was even higher than that measured for the first sample. The reason for the increase in mobility is probably that the carriers in a slab of thickness of 500A are starting to show significant two-dimensional character so that the Fermi energy and velocity for a given doping concentration will be substantially higher than for the thicker slab.

It should be noted that the theory of Read [21] for dislocation scattering suggests that the scattering rate is proportional to the averaged carrier velocity. If the Hall measurements are taken at their face value, the velocities are nearly identical so the scattering rates and mobilities should be very similar for the doped and undoped samples. If on the other hand it is assumed that the Hall measurements grossly overestimate the carrier concentrations in the undoped samples, either because of localisation effects or a p-type layer near to the interface, the carriers in the undoped sample would obey classical statistics at 77K whereas the carriers in the doped sample would be degenerate at this temperature. In this case the Fermi velocity in the doped material would only be a factor of three higher than the averaged velocity for the classical distribution. In both cases it is impossible to explain the very large differences in mobility in terms of the Read theory of scattering from charged dislocations.

It is clear that the Hall measurements obtained with the doped samples are in conflict with those for the undoped samples. Shubnikov-de Haas measurements provide an independent check on both the microscopic carrier concentrations and mobilities in the doped samples. With both samples good quality Shubnikov-de Haas peaks were observed at 4K (see fig seven). In both cases the periods observed at high fields were consistent with the silicon doping levels. Measurements performed with the magnetic field parallel to the slabs showed diamagnetic peaks at fields below 6T due to the emptying of successive subbands. As expected the separation of these peaks increased with decreasing thickness of the slab.

These results demonstrate clearly and unambiguously that the Hall measurements on the thin undoped samples are misleading when interpreted in terms of a single carrier model for InSb grown on GaAs substrates and that the local mobility can be close to the bulk value even when the conducting region is very close to the interface demonstrating that a high density of dislocations has little effect on the electrical properties of the majority carriers. Very similar results are found with thin InAs samples.

The contradictory results for the doped and undoped samples can be reconciled if it is assumed that the apparent catastrophic fall in the mobility in the undoped samples as the film thickness is an artefact arising from the presence of a p-type region close to the interface. The resultant two carrier conduction resulting from such a layer would cause the Hall voltage to decrease rapidly with decreasing thickness while maintaining the local conductivity approximately constant as is observed experimentally with the undoped structures.

The conclusion therefore is that, even when conduction is

confined to within 1000A of the mismatched interface, the high density of dislocations have only a small effect on the carrier mobility. It was shown by Kimmerling & Patel [22] that in silicon only a small proportion of the sites at the dislocation core are electrically active. It therefore implies that virtually all the dislocation core is reconstructed and neutral. Recombination site spacings of the order of 200A along the dislocation cores were estimated. Consequently Kimmerling & Patel proposed that the electrically active sites are located at the dislocation kinks. The situation should be similar in III-V materials [23]. In sufficiently narrow quantum-well superlattice the majority of the dislocation kinks can be expelled from the wells into the barriers with the result that good luminescence efficiency can be obtained from GaAs/AlGaAs quantum well lasers grown on Si substrates [24].

With our thin InSb on GaAs films, a doubly-charged dangling bond at each kink, a kink separation of 200A and a dislocation density of 10^{10} cm^{-2} would give rise to 10^{11} charges cm^{-2} in a 1000A film or a volume density of about $3x10^{16}$ cm^{-3}. This is less than the silicon levels used for the doped InSb samples and therefore in agreement with experiment would not degrade the mobility significantly.

Qualitatively the dislocation structures found in relaxed films of III-V materials on other grossly mismatched substrates appear very similar. Consequently other materials systems such as GaAs or InP on silicon should also show little degradation in the microscopic mobilities even at high dislocation densities.

3.2 Strained Layer Superlattices based on GaAs/InAs

The most extensive studies of strained layer superlattices incorporating strains greater than 1% have been with InAs/GaAs binary and alloy combinations on InP or GaAs substrates (eg. see review by Marzin [25]). Good electrical and optical properties can be obtained at moderate strains (eg. with $Ga_{0.85}In_{0.15}As$ on GaAs, band edge emission showing sharp excitonic peaks can be observed in photoluminescence - see figure eight. The band-edge in these samples can be tuned between 1.3 and 1.4 eV by growing wells of differing thicknesses, thereby changing the confinement energy).

Attempts to grow more strongly strained combinations of GaAs/InAs by MBE have been disappointing. Three dimensional growth is found and indium rich clusters are found in TEM studies. A large shift to lower energy and a degradation of the absorption spectrum is found with such structures (eg. a superlattice structure consisting of two monolayer InAs wells separated by 200A GaAs barriers showed a 100meV wide emission line at 1.15eV- see figure nine).

Recently, however, remarkable results have been obtained by flow-modulation MOCVD growth [26] where the enhanced migration of the In atoms stimulated by the interrupted flow is thought to be responsible for the improved heterostructure quality. Extremely sharp photoluminescence lines (0.4meV full width at half maximum) are seen with InGaAs/GaAs quantum wells grown by this technique. The samples were grown at 500°C.

Even the replacement of a single plane of Ga atoms by In (ie. a single monomolecular well of InAs inserted into a 0.4μm thick GaAs layer) reduces the GaAs band-edge emission in the region of 1.510eV in photoluminescence experiments. The free carriers created in the GaAs diffuse into the InAs monomolecular well and recombine to give a sharp line at 1.483eV of 3meV total width (figure ten). The intensity of this line is some five hundred times greater than the GaAs band edge emission from the same sample and two hundred times stronger than that from GaAs layers grown without the single In plane.

Samples were also fabricated consisting of two InAs monomolecular wells separated by up to 80 GaAs monolayers. With decreasing separation between the wells the emission shifted from 1.483eV to 1.34eV. The observed variation was fitted rather by a simple model which assumed that the electronic wavefunctions were located only in the GaAs (figure eleven) . A significant reduction in the emission wavelength was observed when the number of GaAs planes separating the InAs wells was reduced from one to zero (corresponding to a single InAs two-monolayer well). This result enabled the authors to deduce that the no significant clustering or diffusion of the In was taking place. The reasons for the superior quality of the MOCVD samples compared with those grown by MBE are not clear at the present time.

3.3 Strained Layer Superlattices based on $InSb_{1-x}As_x$

The $InSb_{1-x}As_x$ alloy system exhibits very pronounced band bowing which produces a minimum band gap at a composition of x=0.4 which is much less than the band gap of either InSb or InAs and which corresponds at low temperatures to a wavelength of about 7μm. It has been estimated that by using strained layer techniques it may be possible to reduce the band gap by about a factor of two so that the associated wavelength response would be extended out to 14μm wavelength [27]. However, as discussed in section 2.2, this alloy system is prone to severe structural problems in the mid alloy range. Nevertheless it has proved possible to obtain strained layer superlattice structures with good quantum-well photoemission in the 10μm wavelength region in structures grown by both MOCVD and MBE. A type II superlattice is obtained with x=0.13 and x=0. By varying the period of the superlattice it was possible to use the confinement energy to tune the emission wavelength. As can be seen from figure twelve [13, 28], a sharp photoemission peak corresponding to transitions between the lowest subbands was observed at an energy of 110meV which corresponds to a wavelength of 11.3μm. This system therefore promising for long wavelength detection.

4. The growth of α-Sn and alloys

Tin can be found in nature in the alpha or 'grey' form having diamond structure in addition to its more familiar metallic phase. In a series of pioneering experiments some twenty years ago Paul and other workers [29-31] demonstrated that low impurity concentrations ($<5x10^{14}$ cm^{-3}) and high mobilities ($>10^5 cm^2/Vs$) were achievable with this material. The band structure was of semimetallic form (figure thirteen) giving the possibility that a very small energy gap might be created either by the application of uniaxial stress or by alloying with germanium. However, very little development work was subsequently performed on this material following on the initial demonstration of its electronic properties despite its potential device applicability. The reason for this was the instability of the alpha phase at temperatures above 13°C combined with the relatively difficult preparative techniques involving recrystallisation from liquid mercury solution.

An example of the excellent electronic properties of the material is the dramatic Shubnikov-de Haas effect found at moderate doping levels (figure fourteen) [31]. Several hundred resistance peaks can be observed with samples at carrier concentrations where the Fermi level enters the L-conduction band minima (the indirect band gap in this material is thought to be about 90meV). The appearance of a large number of peaks in the Shubnikov de Haas effect has been interpreted as arising from an enhancement of the screening [32] when the Fermi energy enters the second set of conduction band minima although a decrease in the broadening due to inhomogeneities in the impurity distribution due to the Fermi energy pinning at the L-band energy may have also been playing a role.

Farrow at RSRE Malvern [33] using MBE methods demonstrated two key features of thin-film growth of this material and stimulated a resurgence of interest in its properties. There are currently no less than six groups in the United States engaged in the MBE growth of this material on either InSb or CdTe substrates. We believe that we are the only group outside the USA growing the material by MBE. Strain introduced by growth on a slightly mismatched substrate (such as InSb or CdTe) or by alloying with germanium can stabilise the alpha (diamond structure) phase to above 200°C or above. By chosing the correct combination of alloy composition and substrate it has even been possible to grow InSb on top of a diamond structure Sn/Ge alloy [34] leading to the prospects of superlattices of the alloy combined with InSb. The strain also modifies the band structure opening up a small direct energy gap (figure fifteen). The most direct evidence for the existence of such an energy gap has been the identification of a loss feature in High Resolution Energy Loss Spectroscopy studies [35] for α-Sn samples grown on CdTe substrates. These results and theoretical estimates of the variation of direct energy gap with film thickness are shown in figure sixteen [36]. At thicknesses greater than fifty monolayers the band-gap is determined by the strain and levels off at about 100meV. Quantum confinement increases the band gap to a maximum of about 500meV at 20 monolayers. At smaller thicknesses leakage into the surface regions start to decrease the band gap. A very similar dependence of energy gap on thickness was found from fitting the intrinsic carrier concentration in a series of tin films on CdTe of differing thicknesses [37].

Using a refined substrate cleaning procedures for InSb substrates, we have grown high quality alpha tin layers on InSb which have shown excellent interface properties. A good understanding of the surface reconstruction and growth processes has been obtained by means of RHEED studies [38]. We also are the first group to observe a high mobility two-dimensional electron gas (2DEG) at the interface between the α-Sn and the substrate [39]. Shubnikov-de Haas measurements showed that at least six subbands were occupied (figure seventeen) Rotation of the magnetic field away from the perpendicular to the surface caused the peaks to move upwards in field (figure eighteen) with the $1/\cos\theta$ dependence characteristic of a 2DEG (see Appendix C). Additional peaks due to spin-splitting started to appear at about $\theta=30°$. With the magnetic field applied parallel to the plane of the 2DEG the diamagnetic Shubnikov-de Haas effect could be observed and five subbands were depopulated at fields below 8T (figure nineteen).

The electron concentration concerned is extremely high ($6x10^{12}cm^{-2}$) implying a very high Fermi energy in view of the low effective masses involved. An alternative interpretation that some of the peaks interpreted as individual subbands in figure seventeen might arise from harmonics of lower field peaks which would imply that the total carrier concentration would be very substantially less can be discounted as i) the separation of the peaks in figure seventeen would require that the harmonic content was primarily third harmonic with little or no second harmonic being present ii) a strong harmonic content would be inconsistent with the smooth envelope of the peaks observed in figure seventeen iii) the diamagnetic resonances demonstrate conclusively that a large number of subbands are occupied.

It would therefore seem from the high electron concentration found in the 2DEG that the offsets involved are playing only a minor role in creating the 2DEG. A perfect polar-non polar interface by itself should produce an even higher density of interface charge and the lower carrier density observed may result from deviations from ideality such as the diffusion of one component across the interface. For example the diffusion of Sn by only a single lattice spacing into the InSb would result in an asymmetric δ-doped well in the substrate. Similarly, diffusion of either the In or Sb into the Sn could produce high local doping of the epilayer. The occupancy of the subbands was dependent on the thickness of the tin film indicating that the 2DEG was located at least in part in the tin.

In order to determine whether the effective mass of the two-dimensional carriers could shed further light on whether 2DEG was completely localised in the tin or extended across the interface, magneto-optical experiments were undertaken. In addition to the bound hole transitions from the InSb substrate which extrapolate back to the zero field binding energy of the cadmium acceptors (figures twenty & twenty one), a considerable number of lines could be observed which extrapolated back to the origin indicating that they were cyclotron resonance transitions involving free carriers. The strength of these lines were also extremely dependent on the thickness of the tin film (figure twenty two). With a thin sample a group of lines is observed with effective masses of the order of $0.03m_e$. These are thought to arise from the 2DEG in the interfacial region. With thicker samples the dominant transitions have effective masses in the region of 0.016 to $0.020m_e$. These lines are thought to arise from the strongly non-parabolic and warped energy surfaces in the highly-strained unrelaxed region of the pseudomorphic alpha tin [40].

Low field Hall and conductivity measurements (figure twenty three) show a double reversal of sign of the Hall coefficient as the material is cooled down from room temperature. The reversal at about 130K is due to the freeze-out of intrinsic carriers in the InSb which leaves the substrate p-type at low temperatures. The second reversal is thought to be due to the increasing conductivity of the alpha tin with respect to p-type InSb as the sample is cooled down.

Although the enhancement of the stability of the alpha phase to temperatures of the order of 100°C by growth of thin films on InSb or CdTe has been extremely important, the key to future developments is to increase the stability range even further by alloying the tin with germanium. At first sight this does not seem to be a very promising approach as the alloys are thermodynamically immiscible in the bulk at concentrations of greater than 1% Ge in tin or 2% tin in germanium. Farrow et al [33] were able to observe the stabilising effect of introducing Ge into MBE growth of tin and noted that the bulk immiscibility limit could be overcome. Fitzgerald, Kimerling et al [34] were able to grow good quality metastable films with up to 8% germanium and were subsequently able to extend this to 13% germanium [34]. 1200 A thick films of this composition were stable up to 120-130°C and 50 A films were stable to 220°C. With germanium rich alloys grown on Si substrates, Pukite et al [42] report mirror smooth films stable up to 140°C with a film thickness of 1600 A with 30% of tin and 70% germanium.

5. Atomic Plane, Delta or Spike Doping

Modern epitaxial techniques permit the creation of extremely abrupt doping profiles in the growth direction. The most extreme example of this is atomic plane doping (sometimes referred to as delta or spike doping) where growth is interrupted (usually by switching off the Group III source in the case of III-Vs) and a single plane is flooded with the required dopant. The electronic structure of the doping layer so produced shows a number of striking new quantum features as discussed reference [43].

A major question is whether the dopant can stay localised on the initial deposition plane or whether dopant diffusion or surface segregation occurs. There have been three different approaches to determining this question with the most frequently studied system of silicon donors in GaAs. Firstly the Shubnikov-de Haas effect is extremely powerful in providing very accurate values for the individual subband occupancies (see figure twenty four for. Fourier analysis of Shubnikov-de Haas measurements). The fractional occupancy of the i=0 subband is very sensitive to the diffusion of the dopant as the local potential at the initial doping plane (z=0) loses its cusp-like shape and the effective well broadens and becomes more shallow. Consequently, as can be seen from figure twenty five, the other subbands gain population at the expense of the i=0 subband [44].

In addition the mobility of the carriers in the i=0 subband is rather sensitive to the local potential as these carriers are the most localised in the z-direction. In particular the mobility of the i=0 subband falls as the impurity profile broadens until the width of the dopant region is comparable to the extent of the i=0 wavefunction in the z-direction (typically 30A for GaAs). In the Fourier spectrum shown in figure twenty four the amplitude of the i=0 peak is rather weak because of diffusion of the silicon. However, the mobility of this subband and the amplitude of this peak recover on applying pressure because of the neutralisation of the silicon dopants close to z=0 due to the occupancy of D(X) centres [45].

The other techniques for studying diffusion are capacitance [46,47] and SIMS [48,49] profiling. All three techniques have approximately the same spatial resolution when operating under optimum conditions and, after initial disagreements, there is now a consensus that, provided the silicon concentration does not exceed the bulk solubility equivalent (ie. $6x10^{12}cm^{-2}$) and the growth temperature is kept down to less than or of the order of 500°C in MBE or somewhat higher in MOCVD [50], the silicon remains localised to about 30A or less of the initial doping plane.

Delta doping offers the prospect of building-in extremely high electric fields into structures (approaching $10^6V/cm$) and provides the possibility for a number of new device configurations - see the review in [51]. It also can be used to optimise remote or modulation-doping of heterostructures either to improve the mobility [52] or increase the carrier density [53].

Antimony and arsenic delta doping has also been used very successfully for silicon [54-56] and carrier concentrations well in excess of $10^{13}cm^{-2}$ have been achieved. The mobility is not high enough to enable Shubnikv-de Haas measurements to be informative but several subbands have been detected in tunneling measurements. A short-channel FET structure has also been demonstrated [57].

In our own laboratory Quantum Transport Measurements have been made for single doping planes of silicon donors introduced into InSb and InAs films grown heteroepitaxially onto GaAs substrates by MBE. Up to five subbands are occupied (figures twenty six and seven). The free electron concentration saturates at carrier concentrations of $4x10^{12}cm^{-2}$ in the case of InSb but a concentration of $2x10^{13}cm^{-2}$ is achieved with InAs [58]. Good agreement is achieved between the individual subband carrier concentrations deduced from Fourier analysis of Shubnikov-de Haas measurements and the calculated occupancies indicating that the diffusion of the silicon was small (≤ 50A) although in the case of InSb significant diffusion could be detected if the growth temperature was greater than about 340°C. Figure twenty six shows the shift downwards of the i=0 peak and the characteristic reduction in amplitude due to the drop in subband mobility arising from dopant diffusion which were seen in the results for GaAs (figures twenty four and five).

The diamagnetic Shubnikov-de Haas peaks observed with these materials when the magnetic field is applied parallel to the doping plane were in the predicted positions (see figure twenty eight and Appendix C1).

6. Doping Superlattices & N-I-P-I Structures

N-i-p-i doping superlattices offer one of the most flexible approaches to the tailoring of the optical properties of materials near to or below the band gap [60,61]. Band-gap tuning, strong optical nonlinearities and greatly enhanced carrier lifetimes have all been reported (although the latter is accompanied by a decreased absorption coefficient). Figure twenty nine shows the change in the photoluminescence as a function of pump power which is characteristic of a n-i-p-i structure [62]. The structure is a a GaAs short-period ('type A') superlattice where the recombination time is relatively short and the band-gap is reduced by about 40% due to the saw-tooth doping potential. At low pump powers there is virtually no emission at the normal GaAs band edge wavelength of 850nm but instead a strong series of lines are observed which arise from transitions between different subbands in the n-i-p-i structure [63]. As the pump power is raised to an intermediate level these lines all shift to shorter wavelength because the saw-tooth potential is partiallyu screened by the photoexcited carriers. At the highest power levels the band edges have virtually straightened out because of the large number of photoexcited carriers present and virtually all the emission is at the GaAs band edge.

A GaAs laser structure incorporating a n-i-p-i region has been reported to be tunable over a wavelength range of 35A [64] and an all GaAs technology for the minimum dispersion region of silicon fibres (1.3μm) based on n-i-p-i devices has been proposed [65].

N-i-p-i structures can also show unusual electronic properties also. Long period (type B) structures show a very pronounced negative differtential conductance in perpendicular transport measurements although short period (type A) structures show a linear J-V characteristic because of tunneling through the thin barriers [66].

Perhaps the spectral region which has the most potential for n-i-p-i structures is the mid-infrared [68-70]. In our laboratory we have grown n-i-p-i structures in both InSb and InAs. With heavily doped n-i-p-i superlattices the silicon doping achieved for both materials was consistently 25% greater than anticipated which is suggestive that the dopant incorporation is dependent on the Fermi energy. Local vibrational mode studies on GaAs [67] showed that incorporation of silicon on the gallium site could be very substantially improved when the material was codoped with beryllium demonstrating that the position of Fermi level was crucial in determining the silicon site distribution as would be expected from the ideas associated with amphoteric native defects discussed earlier [3-5].

Careful control of doping can be used to produce asymmetric n-type n^+-i-p-i structures designed to reduce the number of subbands occupied for a given carrier concentration in each n-type well. Such structures showed very pronounced Quantum Hall plateaux (see figure thirty). These structures have potential application for photodetection based on intersubband transitions where ideally all carriers should be located in the lowest (i=0) subband.

Our InSb n-i-p-i structures have shown all of the characteristic optical properties expected of such structures (ie. long recombination times, strong subband-gap absorption and strong optical nonlinearities in the subband-gap region) [68] - see also figure thirty one. Detectivities (D^*) values of $8x10^{10}cm\sqrt{Hz}$ are anticipated [69].

7. Intersubband Quantum Well Detectors

Electromagnetic transitions between the size-quantised subbands in quantum wells have been proposed as the basis for infrared detection. In order for there to be a matrix element the radiation must be polarised with the electric field vector perpendicular to the plane of the well which is experimentally inconvenient but can be achieved by grating coupling or introducing the radiation from the side in a waveguide geometry. Oblique incidence can also be employed but this has low efficiency because of the large refractive indices of common semiconductors. With GaAs quantum wells the 10μm region can be covered and detectivities of about $10^{10}cm\sqrt{Hz}/W$ have been reported [71]. Advantage could also be taken of the mature GaAs growth and processing technologies giving the prospect of integration with high-speed FETs and enabling large area focal plane arrays of detectors to be considered.

However the detectivities achieved are still far less than the industry standard system which is $Hg_{1-x}Cd_xTe$ where detectivities of $3x10^{12}cm\sqrt{Hz}/W$ are possible at 77K [72]. Furthermore the technology for HgCdTe is now extremely well advanced and, by using non-equilibrium depletion techniques to suppress Auger noise, it is now possible to achieve comparable detectivities close to room temperature 73].

It should be possible by going to more refined structures such as those using grating enhancement [74] or exploiting Fabry-Perot structures [75] to improve the performance of intersubband detectors.

Generally a sharply-peaked response is observed (typically 6meV or about 50 cm^{-1} full width for the i=0 to 1 transition in GaAs (fig. 32) [76,77] with more than double this width being found with InGaAs wells [78,79]). If interpreted as a natural width 6meV would correspond to a lifetime of 0.1ps. However saturation experiments give decay times of up to 15ps [80]. Thus the observed line-width probably arises from variation in well width.

8. Acknowledgements

The work and assistance of the following past and present members of Imperial College is gratefully acknowedged: R. Droopad, J. Ferguson, C.C. Hodge, E.J. Johnson, B.A. Joyce, W. Liu, A. MacKinnon, R. Newman, A.d'Oliveira, S.D. Parker, S. Patel, C.C. Phillips, P.D. Wang, R.L. Williams, W.T. Yuen. and Z. Wasilewski.

Conversations with H. Kroemer, J. Merz and W. Walukiewicz were extremely helpful in assisting my understanding of the electrical properties of dislocations and the properties of native defects and interfaces and conversations with R. Booker, A. Norman & T. Seong on the structural properties of alloys and for the gift of the TEM micrograph shown in figure five are also gratefully acknowledged.

FIGURE CAPTIONS

Figure One shows the magneto-optical spectrum of an MBE sample of InAs. The sharp lines are free carrier cyclotron resonance and the donor transitions from the bulk region of the sample. The broad line is from a two dimensional electron gas at the surface of the sample. The sample is tilted with respect to the magnetic field so the cyclotron resonance from the 2DEG is moved up in field with respect to the cyclotron resonance of the bulk carriers. From ref. [1].

Figure two shows the predicted position of the amphoteric native defect discussed by Walukiewicz [4] with respect to band edges of various III-V compounds. In all cases except InAs this level occurs in the forbidden band gap.

Figure three shows the predicted effects of parallel conduction as a function of thickness for a two-carrier layered system consisting of a low-mobility high-carrier concentration surface skin and a high-mobility low-carrier concentration bulk region. The curves show the predicted Hall mobility and apparent carrier concentration of such a sample as a function of thickness. The symbols are experimenta. Hall data for MBE InAs at 77K. Th values of n and μ used to generate the solid curves are derived from magneto-optical experiments. For such a system Hall measurements at 77K will only give the true bulk values of n and μ for thicknesses ≥ 20μm and if fields ≤ 0.01T are employed so that the low-magnetic-field limit is attained (taken from ref [1]).

Figure four shows the variation of Hall mobility and carrier concentration for a series of $InAs_{1-x}Sb_x$ alloy samples prepared by MBE. The upper set of points are for films grown at 410°C, the lower for samples grown at 370°C. The lower set of samples exhibit the phase separation effects shown in figure five for compositions ($0.2 \leq x \leq 0.8$) (I. Ferguson, A. d'Oliveira & R.A Stradling to be published).

Figure five shows the platelet structure due to phase segregation observed in transmission electron microscopy for a sample of InAsSb (photo courtesy of T. Seong)

Figure six shows the Hall mobility and carrier concentration measured for a range of InSb on GaAs heterostructures of differing thicknesses (S.J. Patel - MSc thesis, Imperial College).
Δ Magnetron Sputtered Sample [Zaj]

Figure seven shows Shubnikov-de Haas oscillations observed with a thin doped sample of InSb grown on GaAs. The measured mobility increased by three orders of magnitude in this sample compared with an undoped sample of the same thickness.

Figure eight shows the 77K absorption spectra of a series of $Ga_{0.85}In_{0.15}As$ superlattices where the quantum well thickness is varied from sample to sample (from ref.[25]).

Figure nine shows the photoluminescence emission spectrum for an ultrathin quantum well structure consisting of two monolayers of InAs in GaAs grown by MBE (from ref. [25]).

Figure ten shows the photoluminescence emission spectrum for a structure consisting of a single monolayer of InAs in GaAs grown by a flow-modulation MOCVD technique (from ref. [26]).

Figure eleven shows the energy of the main photoluminescence emission line in structures consisting of two single monolayers of InAs in GaAs grown by a flow-modulation MOCVD technique (from ref. [26]). The figure shows the variation in the energy as a function of separation of the two monolayers. The full line is the predicted variation.

Figure twelve shows the photoemission from two strained layer superlattices consisting of $InAs_{0.15}Sb_{0.85}/InSb$ multiple quantum wells. The emission between the lowest subbands is at a wavelength of 11.3μm for the structure with the wider wells (260A repeat distance) from ref.[11].

Figure thirteen shows the band structure proposed for alpha-tin (after ref. [29]).

Figure fourteen shows the Shubnikov-de Haas effect observed with a bulk sample of alpha-tin prepared from recrystallisation from mercury (from ref. [32])

Figure fifteen shows the band structure of alpha tin under uniaxial compressive and tensile stress [40].

Figure sixteen shows the theoretical and measured variation in band gap as a function of film thickness for α-Sn samples grown on CdTe substrates [35,36].

Figure seventeen shows the Fourier analysis of the perpendicular field Shubnikov-de Haas effect for an epitaxial α-Sn sample grown on InSb. Up to seven subbands are occupied [39].

Figure eighteen shows the effect on the Shubnikov-de Haas peaks of tilting the magnetic from the perpendicular orientation with respect to the surface of a heterostructure of α-Sn on InSb. The peaks move upwards in field as $1/\cos\theta$ until at $\theta = 30°$ additional structure is seen due to spin-splitting.

Figure nineteen shows the diamagnetic Shubnikov-de Haas resonances observed with the magnetic field applied parallel to the plane of an α-Sn on InSb heterostructure [39].

Figure twenty and twenty one shows the farinfrared magneto-optical transitions observed with an α-Sn on InSb heterostructure taken at wavelengths of 70 and 96 μm. The lower recording in the top set is for bulk p-InSb and the strong sharp lines are acceptor transitions. Curves b) and c) are for two α-Sn

films of differing thickness and d) a for a similar specimen except that the α-Sn has been etched away. The broad lines at about 2.5T clearly arise from the tin film. In the lower set of recordings taken at the longer wavelength the acceptor transitions have moved to lower field revealing a complicated series of lines for the two samples with differing thicknesses of tin.

Figure twenty two shows a fan chart of the bound acceptor transitions in InSb illustrating how the lines arising soleley from the InSb move with wavelength (energy) as seen in figures twenty and twenty one.

Figure twenty three shows the results of low field Hall and conductivity measurements for an α-Sn/InSb heterostructure.

Figure twenty four shows the results of Fourier analysis of the de Haas-Shubnikov effect in a delta doped sample of GaAs for a number of different values of hydrostatic pressure. The i=0 subband is moved down in field (N_s) and is weak at zero pressure. These features are characteristic of the silicon dopant diffusing a distance comparable with the extent of the i=0 wavefunction. On applying pressure DX centres become occupied close to the z=0 plane and consequently the mobility of the highly localised i=0 subband and the amplitude of the Shubnikov-de Haas effect for this subband improve - from ref. [45].

Figure twenty five shows the shift in energies of the subbands in planar doped GaAs as a function of the width of the doping slab (courtesy E.J. Johnston & A. MacKinnon see also ref [59]).

Figure twenty six shows the results of Fourier analysis of the de Haas Shubnikov effect in atomic plane doped InSb. The upper recording is for a sample grown at 340°C and the i=0 subband is shifted to lower field (occupancy) and is weaker compared with the results for the sample grown at 240°C (lower recording). The features are characteristic of the silicon dopant diffusing at the higher temperature from ref [58].

Figure twenty seven shows the results of Fourier analysis of the de Haas-Shubnikov effect in atomic plane doped InAs from ref [58].

Figure twenty eight shows a fan-chart of the positions of the diamagnetic resonances in planar doped InSb on a reduced field-occupancy plot to demonstrate the universality of the results for different materials; from ref [58], see also Appendix C

Figure twenty nine shows the photoluminescence from a short-period GaAs n-i-p-i structure as a function of the laser pump power demonstrating strong sub band-gap luminescence at low power levels. These lines progressively shift and bleach with increasing power until at high power levels the GaAs band edge emission is seen - from ref [64].

Figure thirty shows the pronounced Quantum Hall Effect arising from carriers in a single spin-split subband in an InSb n+-i-p-i structure. In single delta wells up to six subbands are occupied (see fig twenty six) and consequently the Quantum Hall Effect is very weak in such structures.

Figure thirty one shows the characteristic photoresponse below the band edge expected for a n-i-p-i structure. The sample was grown by MBE at Imperial College - from ref. [68].

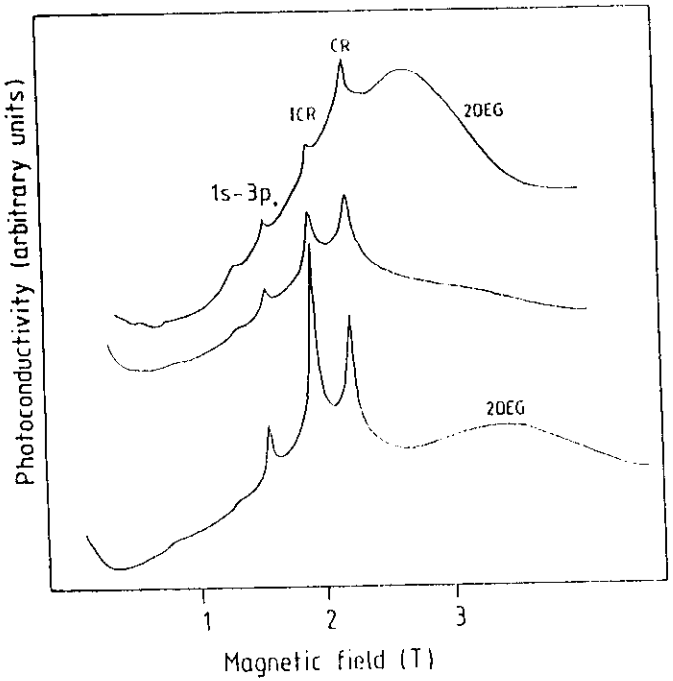

Fig. 1

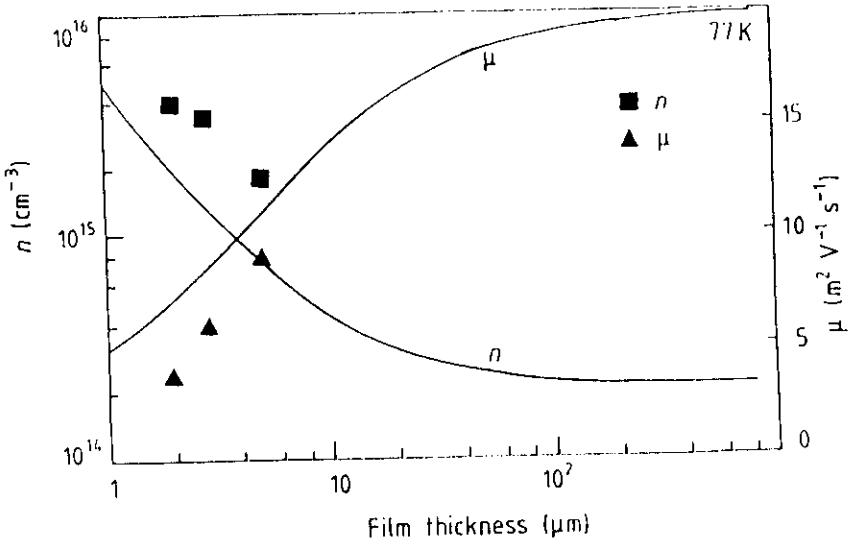

Fig3

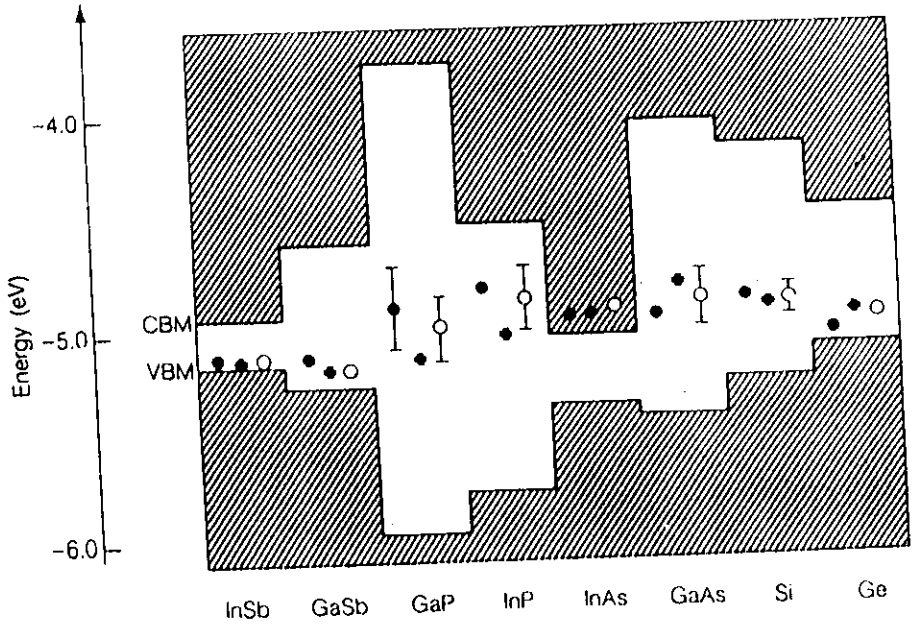

Fig. 2

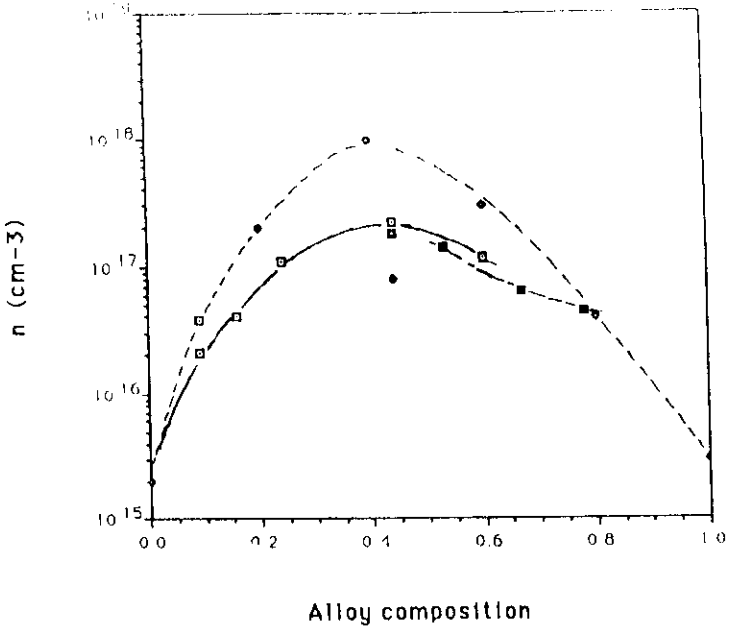
n (cm-3)
10 18
10 17
10 16
10 15
0 0
0 2
0 4
0 6
0 8
1 0
Alloy composition


002
100nm
InAs.4Sb.6

Fig.5

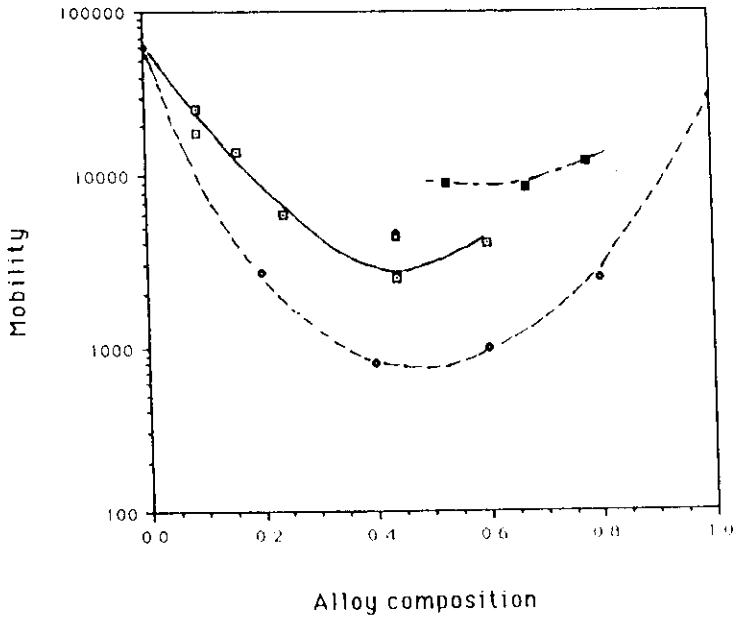
Mobility
100000
10000
1000
100
0 0
0 2
0 4
0 6
0 8
1 0
Alloy composition

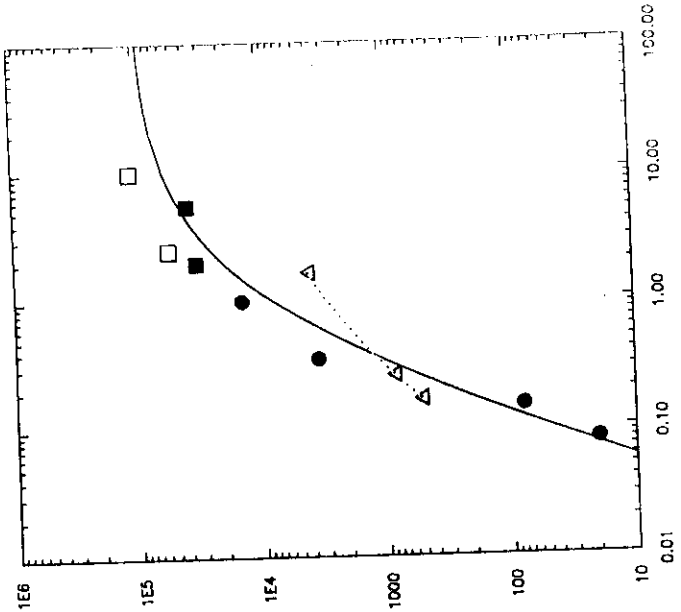
1E6
1E5
1E4
1000
100
10
100.00
10.00
1.00
0.10
0.01

fig.6

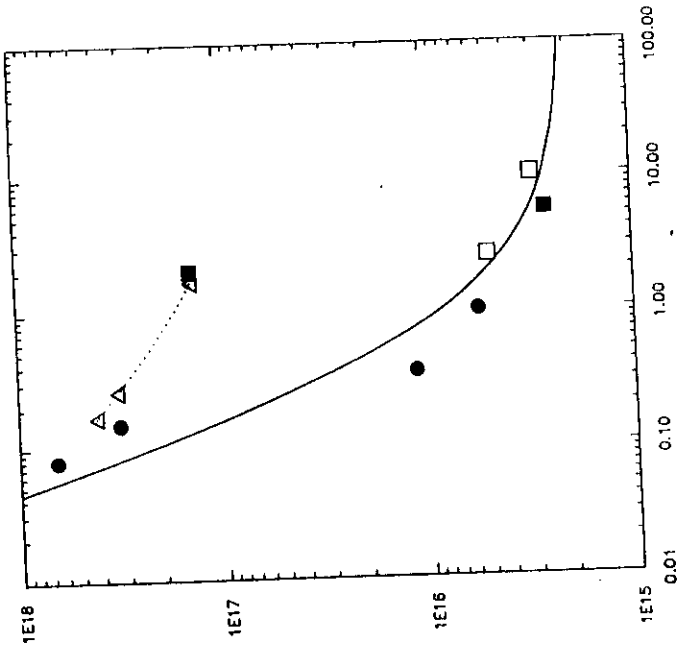
1E18
1E17
1E16
1E15
100.00
10.00
1.00
0.10
0.01

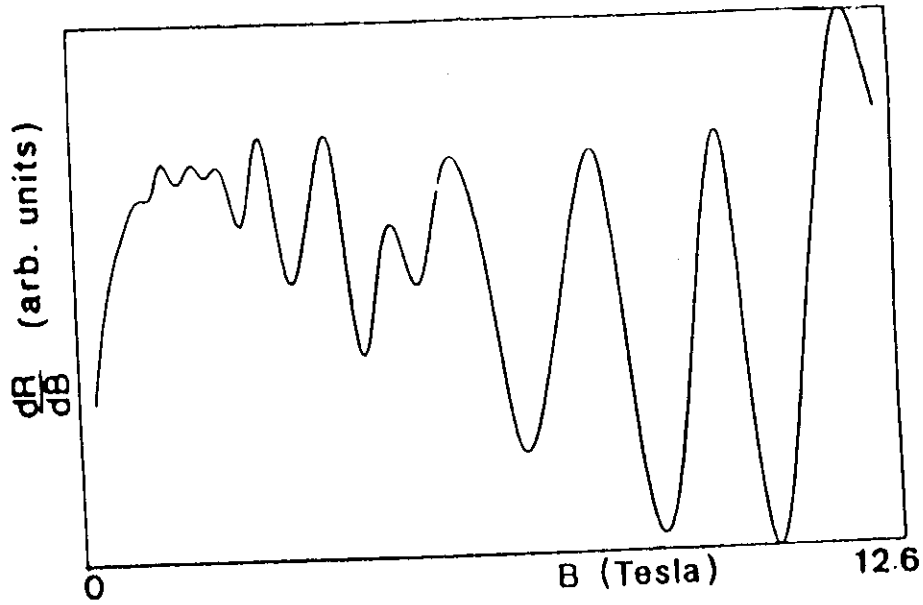
dR/dB (arb. units)
0
B (Tesla)
12.6

Fig.7

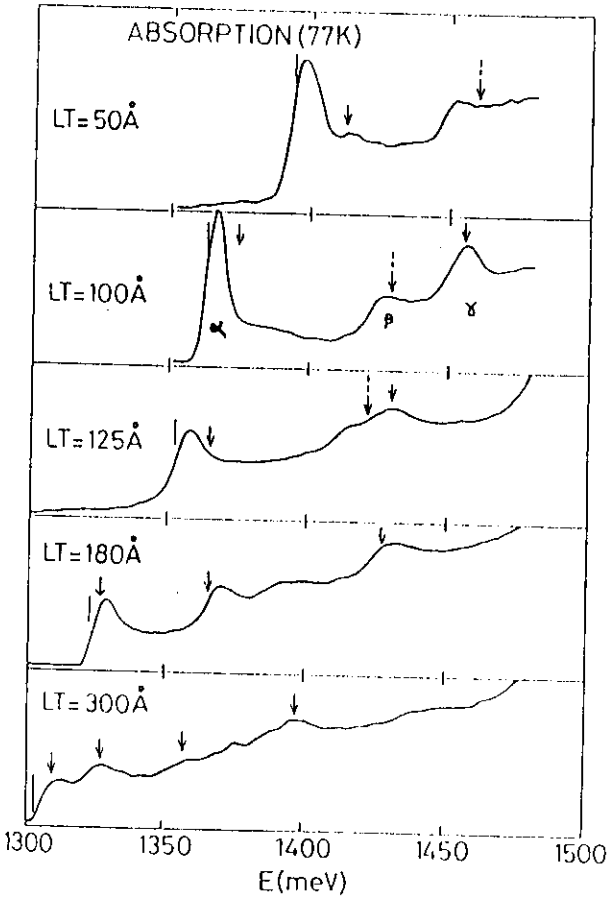

Fig. 8

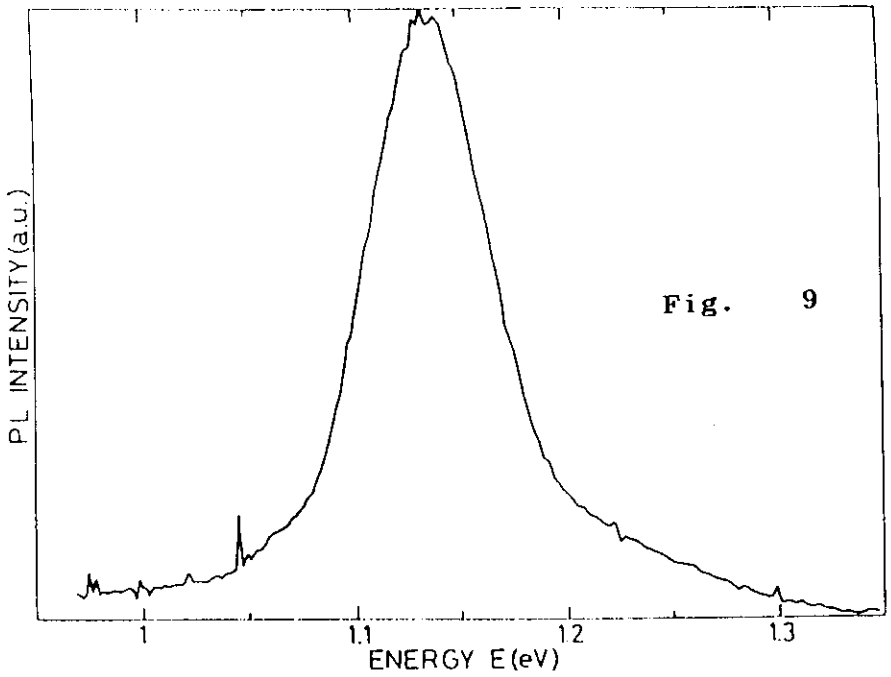

Fig. 9

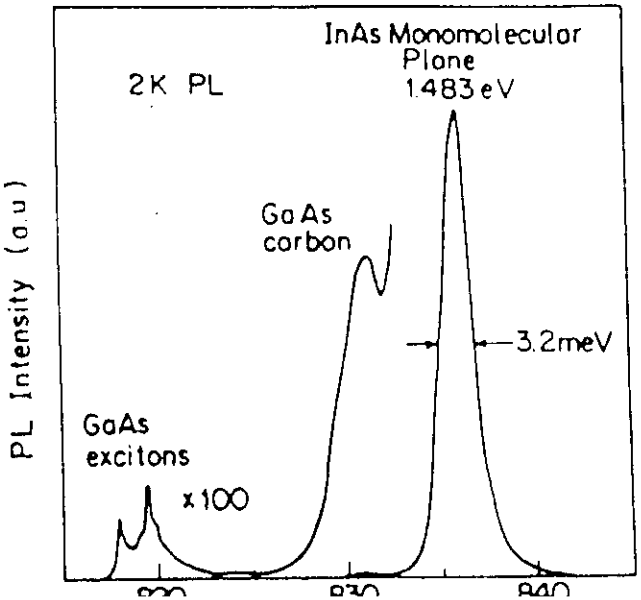

Fig. 10

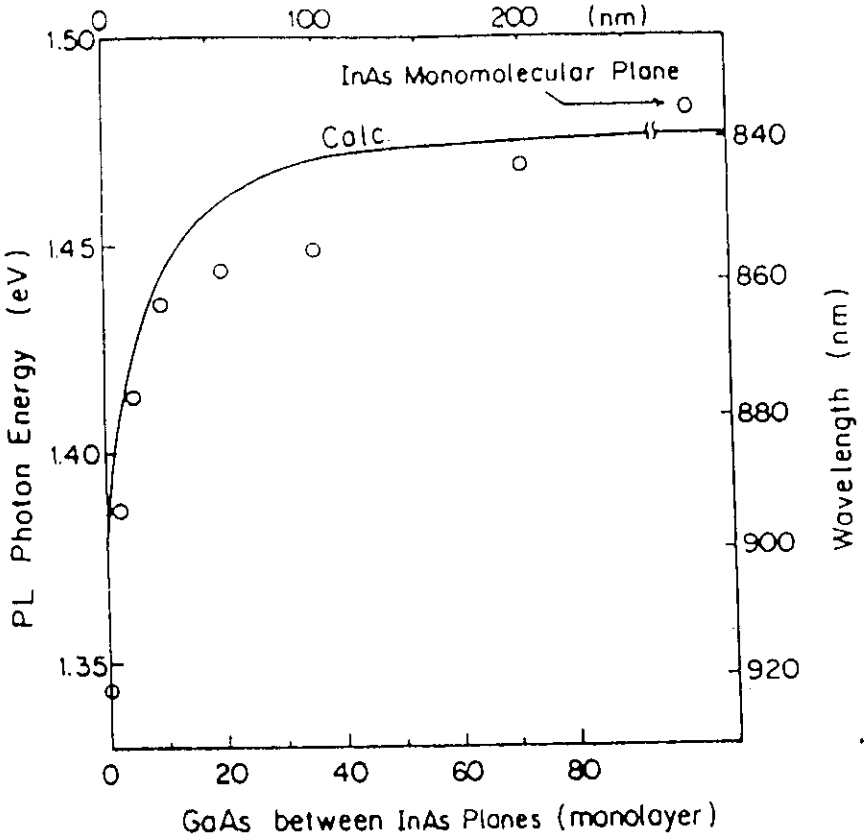
0
100
200
(nm)
1.50
InAs Monomolecular Plane
Calc.
840
1.45
860
880
1.40
900
1.35
920
PL Photon Energy (eV)
Wavelength (nm)
0
20
40
60
80
GaAs between InAs Planes (monolayer)

Fig. 11

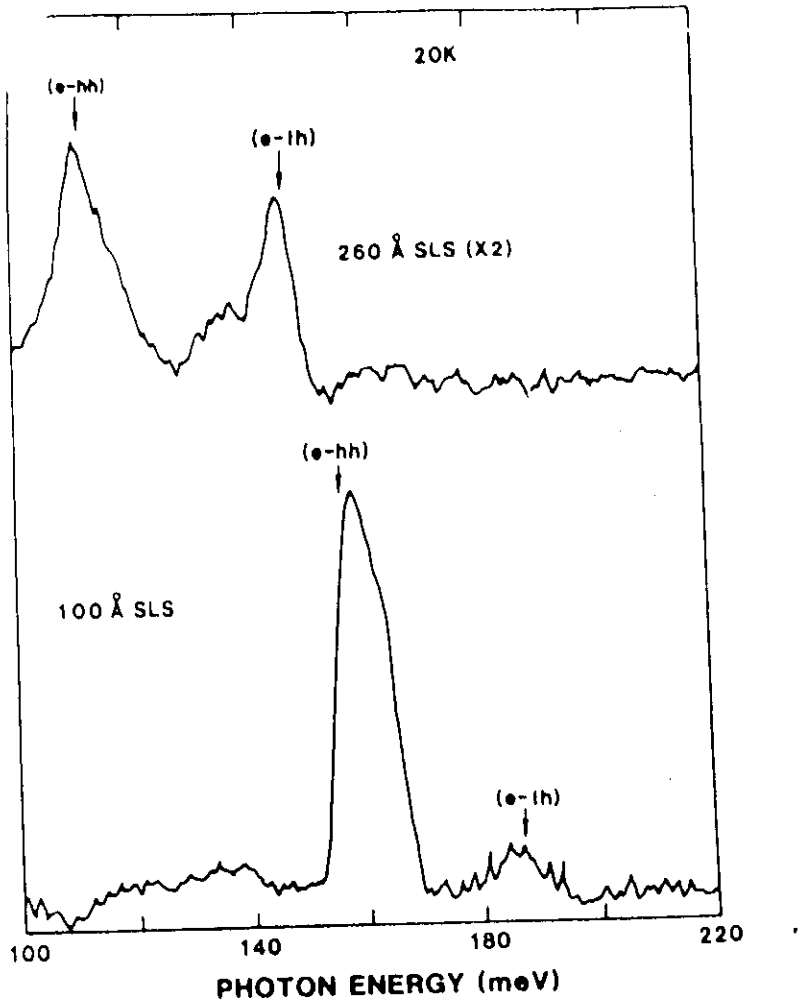
20K
(e-hh)
(e-lh)
260 Å SLS (X2)
(e-hh)
100 Å SLS
(e-lh)
100
140
180
220
PHOTON ENERGY (meV)

Fig. 12

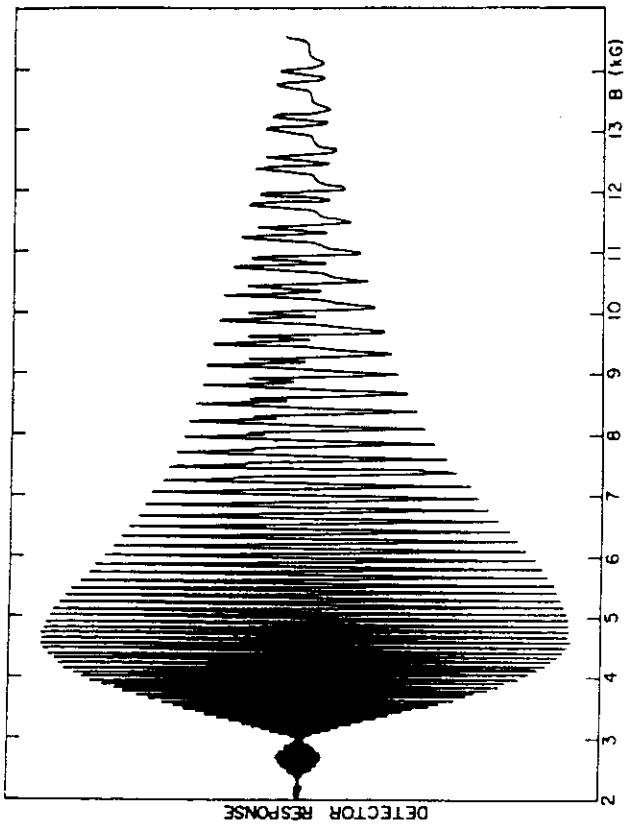

Fig. 14

B & B model
Eg = 0.35eV
Eg' = 0.4eV

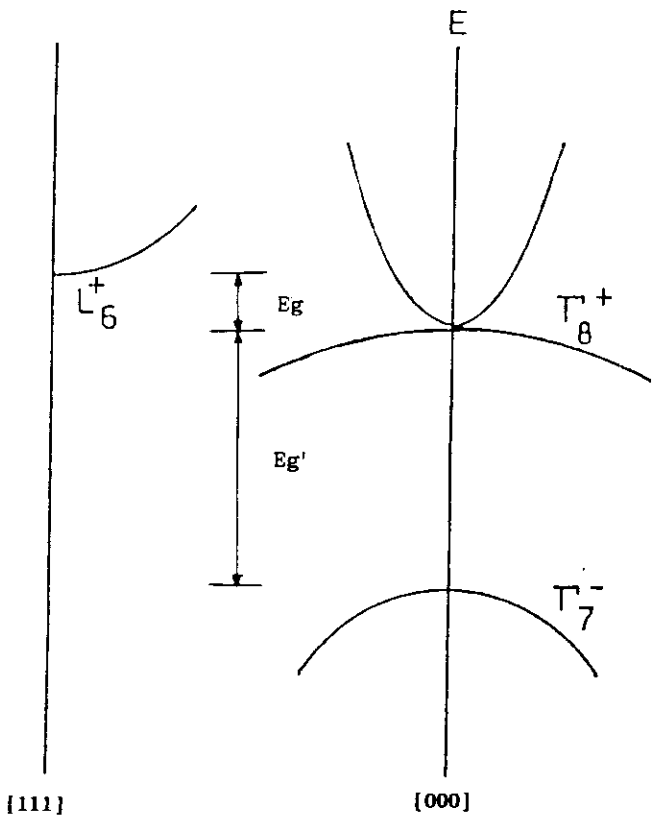

G & P model
Eg = 0.09 eV
Eg' = 0.41 eV

Fig. 13

Sketch of the energy-band structure of alpha-Sn near the center of the Brillouin zone.

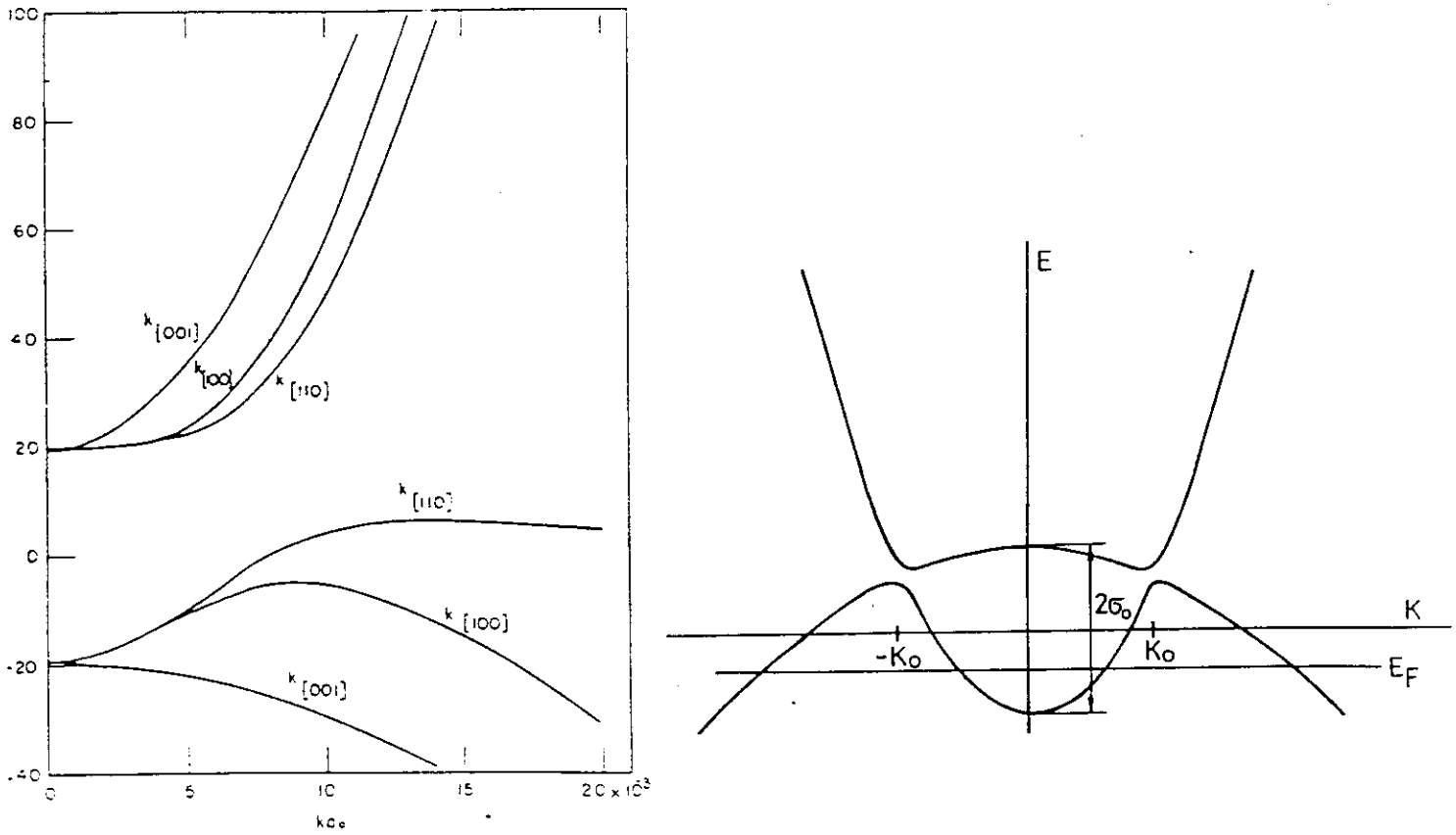
100
80
60
40
20
0
-20
-40
0
5
10
15
20 x 10³
k[001]
k[100]
k[110]
k[110]
k[100]
k[001]
E
2σ₀
K
-K₀
K₀
E_F

Fig. 15

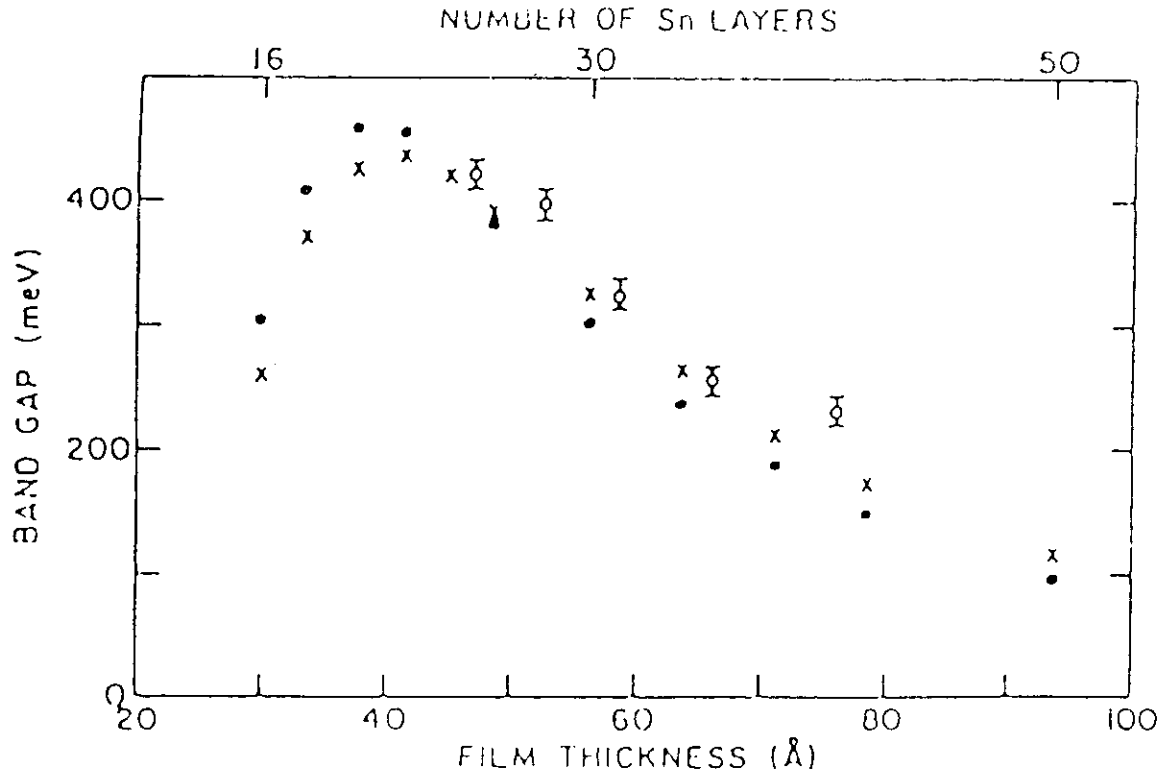
NUMBER OF Sn LAYERS
16
30
50
400
200
0
BAND GAP (meV)
20
40
60
80
100
FILM THICKNESS (Å)

Fig. 16

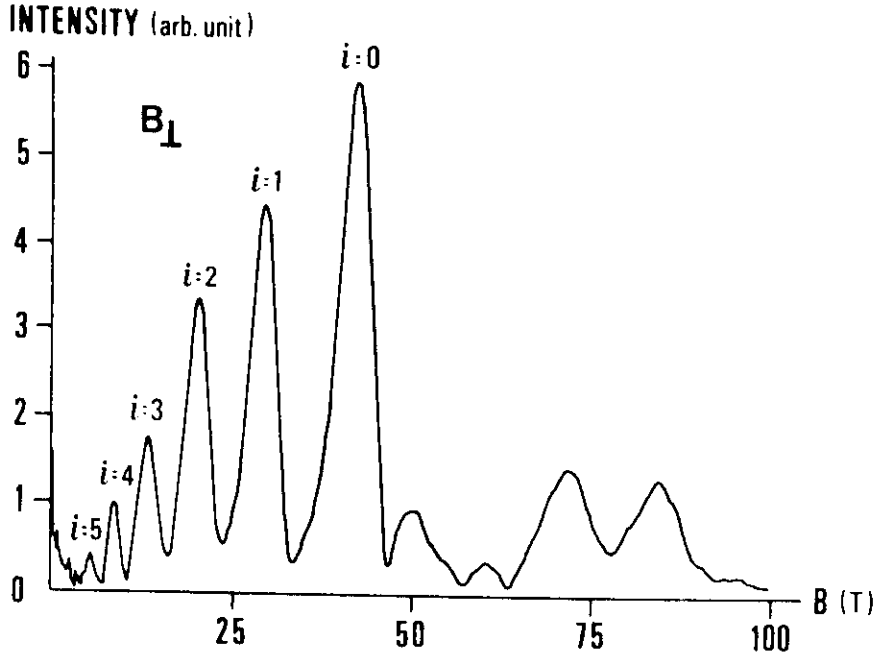
INTENSITY (arb. unit)
6
5
4
3
2
1
0
$B_\perp$
i:0
i:1
i:2
i:3
i:4
i:5
25
50
75
100
B (T)

Fig. 17

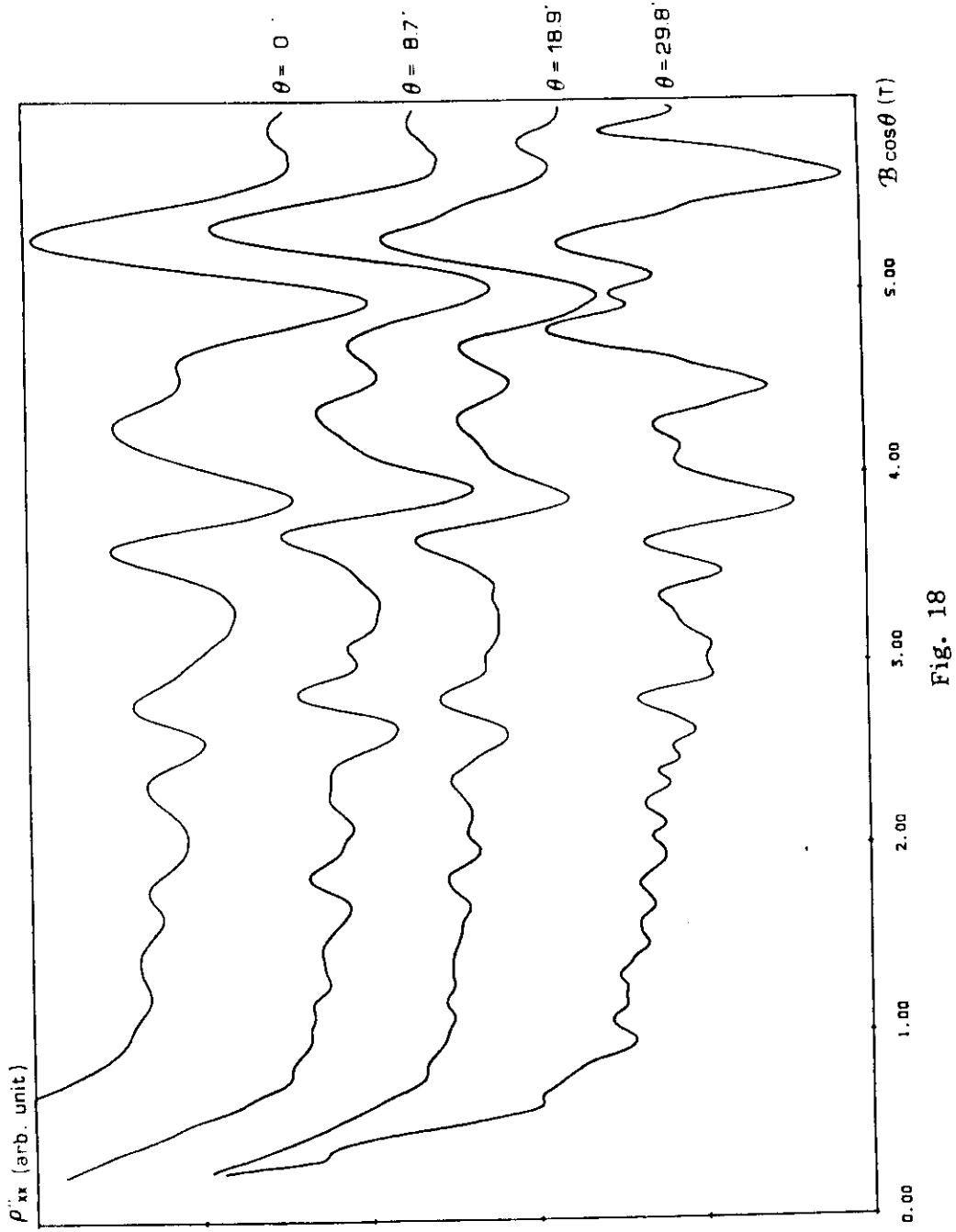
θ = 0°
θ = 8.7°
θ = 18.9°
θ = 29.8°
ρ'_{xx} (arb. unit)
$B\cos\theta$ (T)
0.00
1.00
2.00
3.00
4.00
5.00

Fig. 18

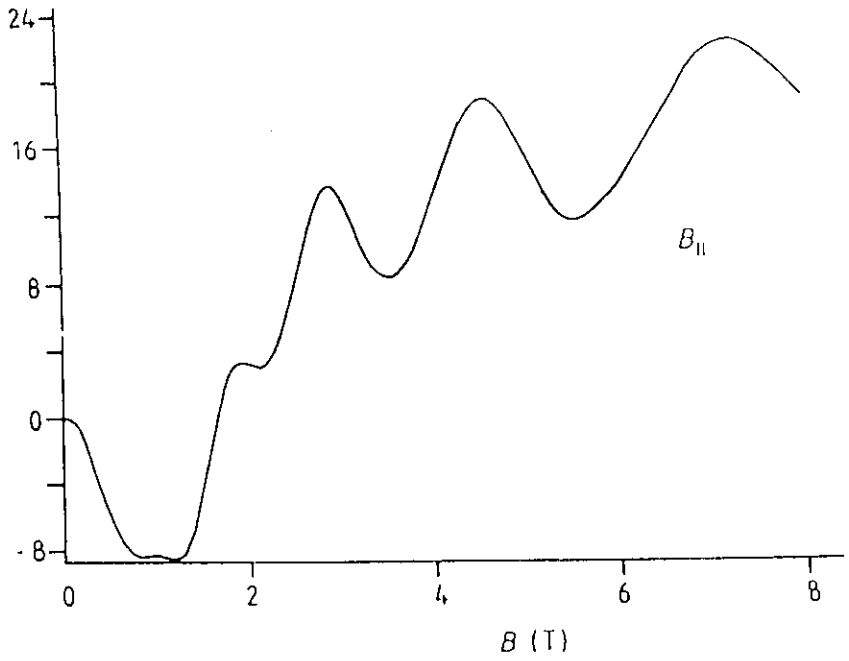
24
16
8
0
-8
0
2
4
6
8
B (T)
$B_{\perp}$

Fig.19

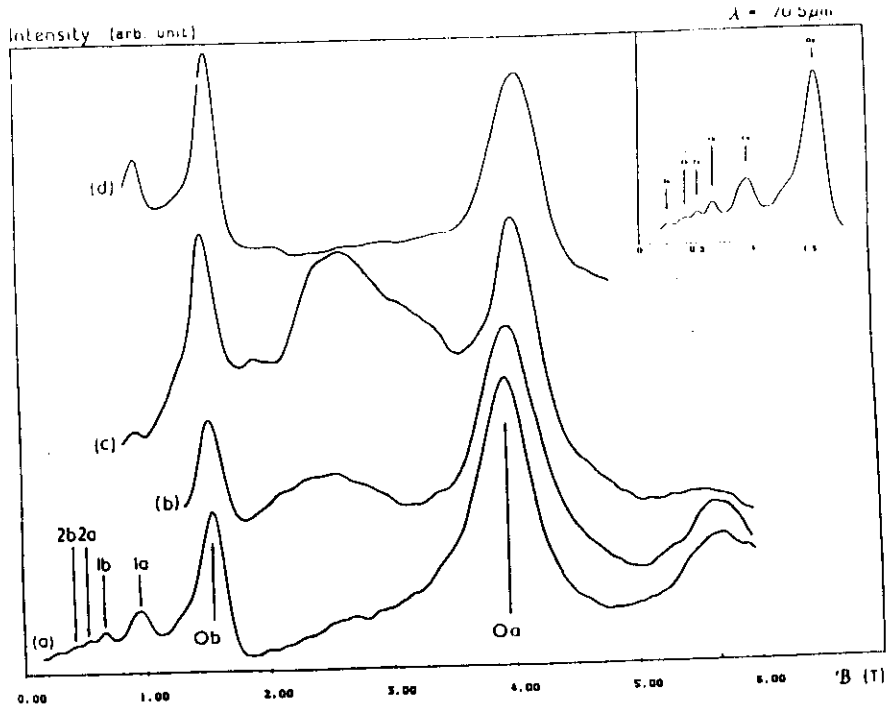
Intensity (arb. unit)
(d)
(c)
(b)
(a)
2b 2a
1b
1a
Ob
Oa
0.00
1.00
2.00
3.00
4.00
5.00
6.00
B (T)

Fig. 20

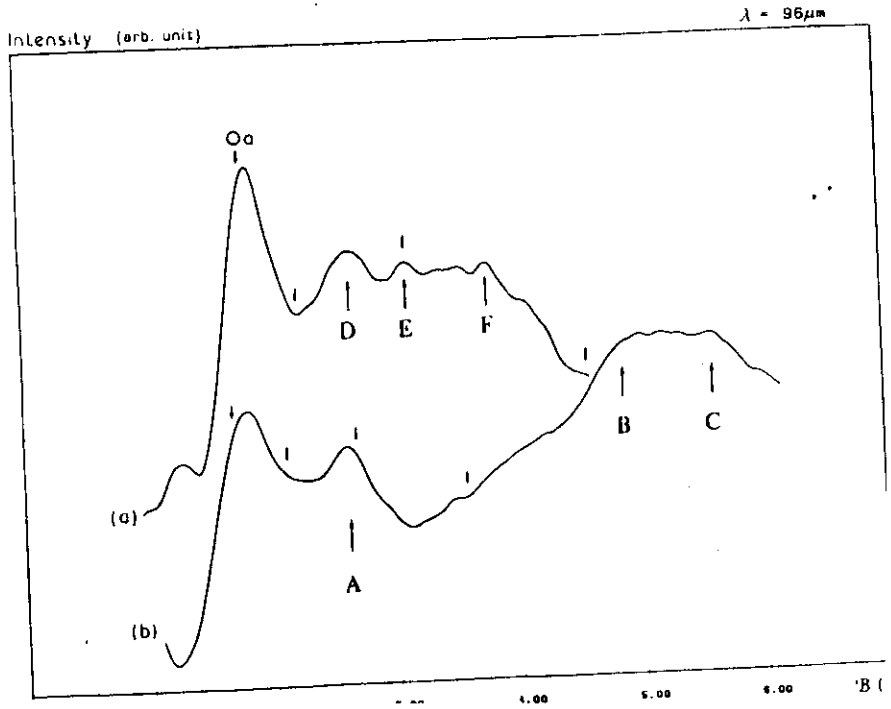
Intensity (arb. unit)
Oa
D
E
F
B
C
A
(a)
(b)
5.00
6.00

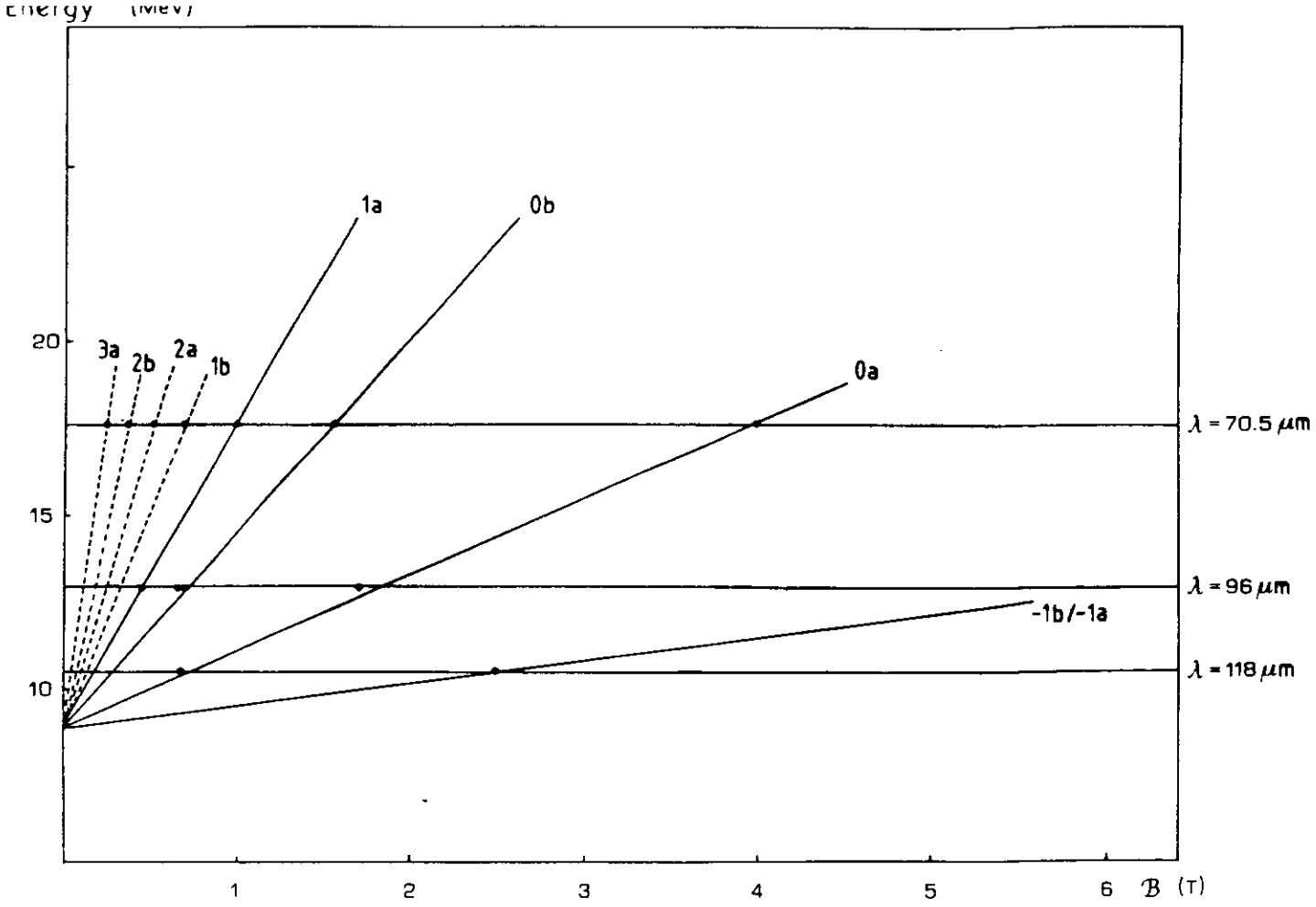
Energy (MeV)
20
15
10
3a
2b
2a
1b
1a
0b
0a
-1b/-1a
λ = 70.5 μm
λ = 96 μm
λ = 118 μm
1
2
3
4
5
6
B (T)

Fig. 22

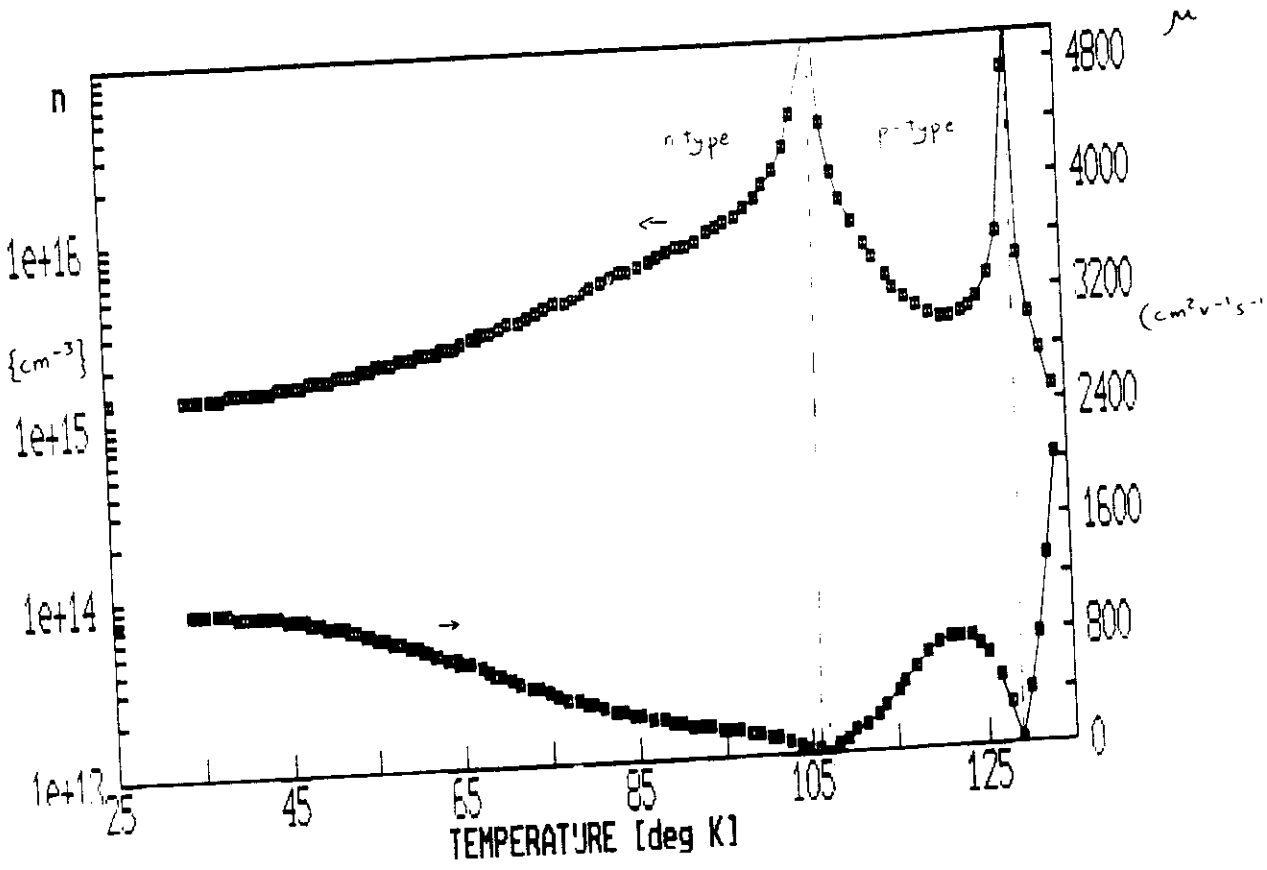
n
1e+16
{cm⁻³}
1e+15
1e+14
1e+13
n type
p-type
4800
4000
3200
2400
1600
800
0
(cm²v⁻¹s⁻¹
25
45
65
85
105
125
TEMPERATURE [deg K]

Fig. 23

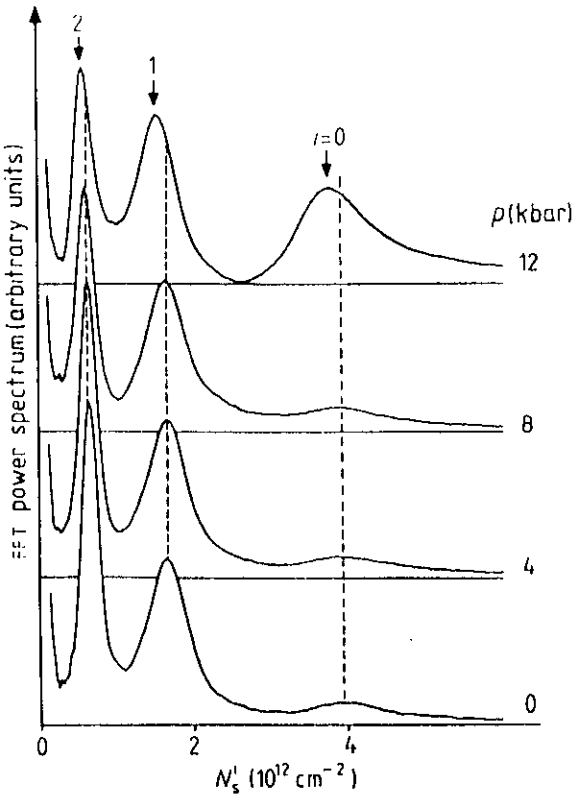
2
1
i=0
p(kbar)
12
8
4
0
FFT power spectrum (arbitrary units)
0
2
4
N_s' (10^{12} cm^{-2})

Fig. 24

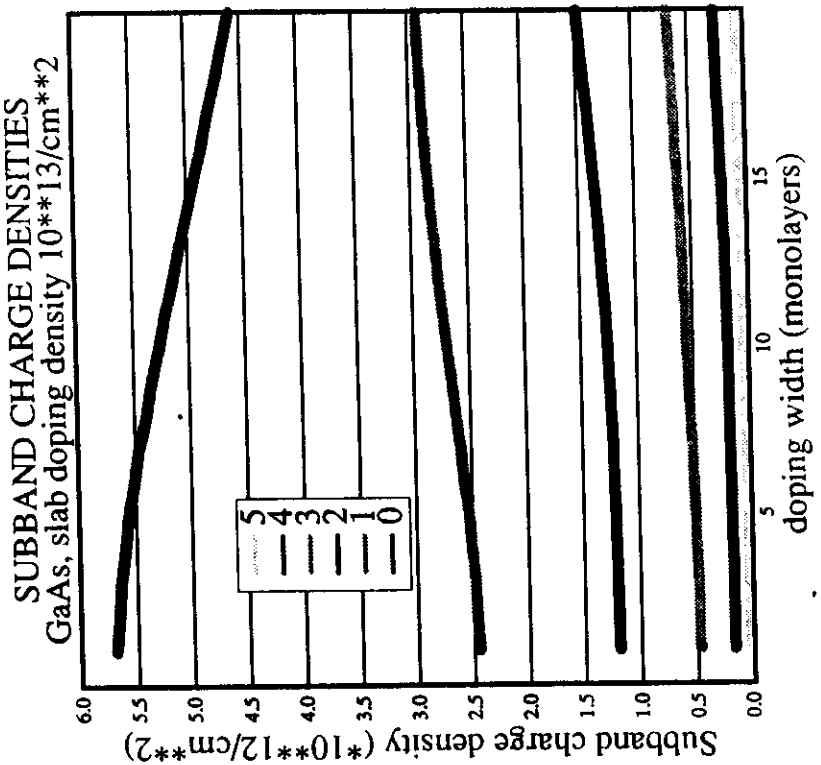
SUBBAND CHARGE DENSITIES
GaAs, slab doping density 10**13/cm**2
5
4
3
2
1
0
Subband charge density (*10**12/cm**2)
6.0
5.5
5.0
4.5
4.0
3.5
3.0
2.5
2.0
1.5
1.0
0.5
0.0
5
10
15
doping width (monolayers)

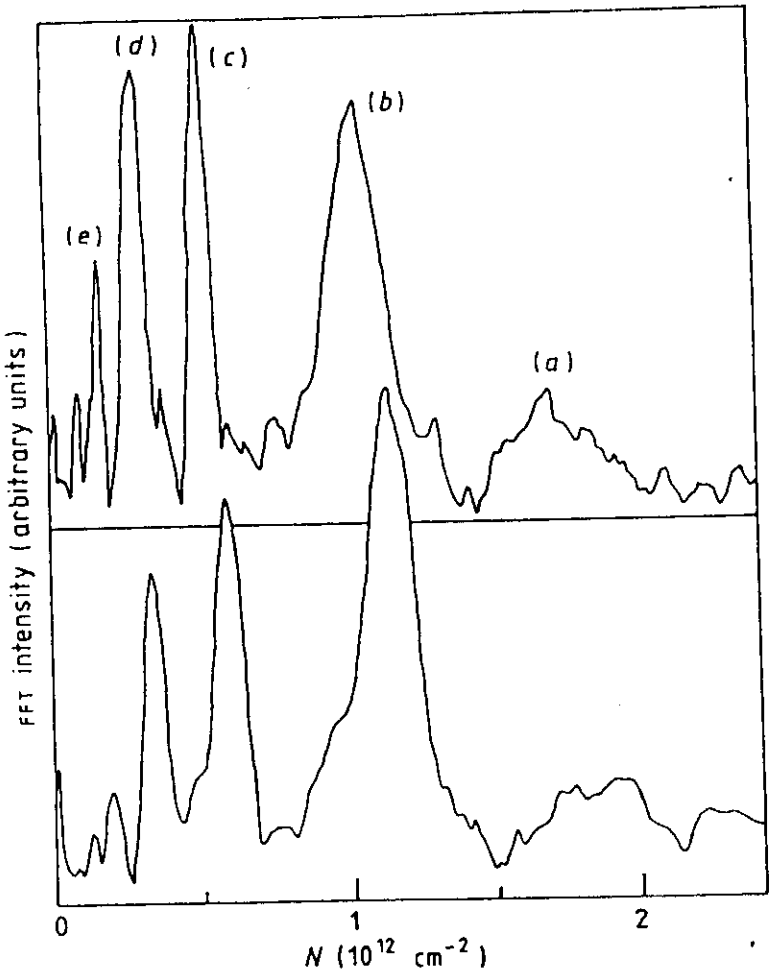

Fig. 26

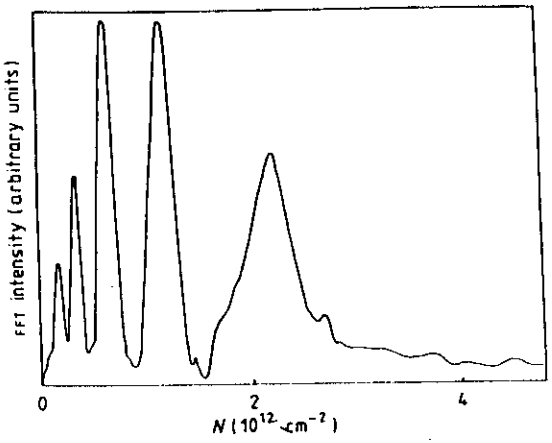

Fig. 27

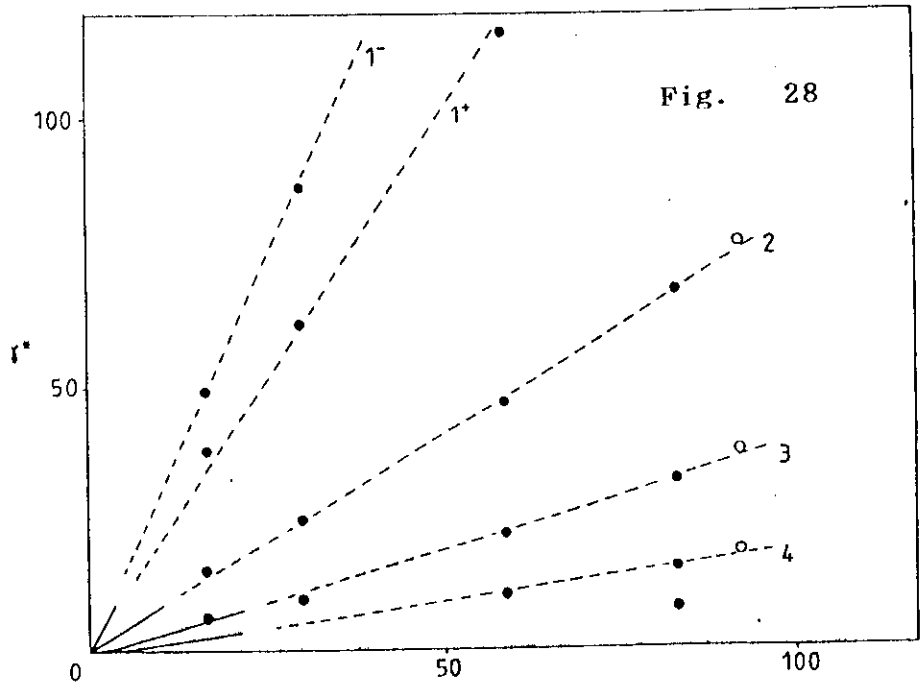

Fig. 28

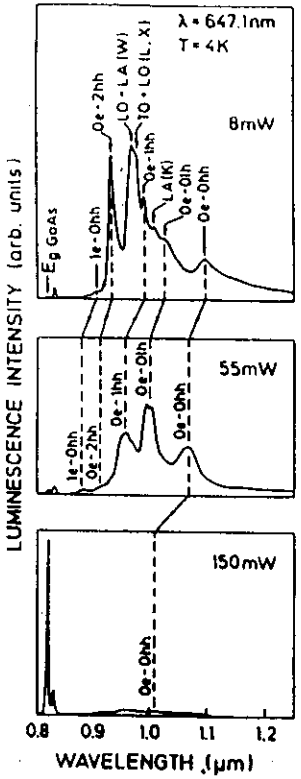

Fig. 29

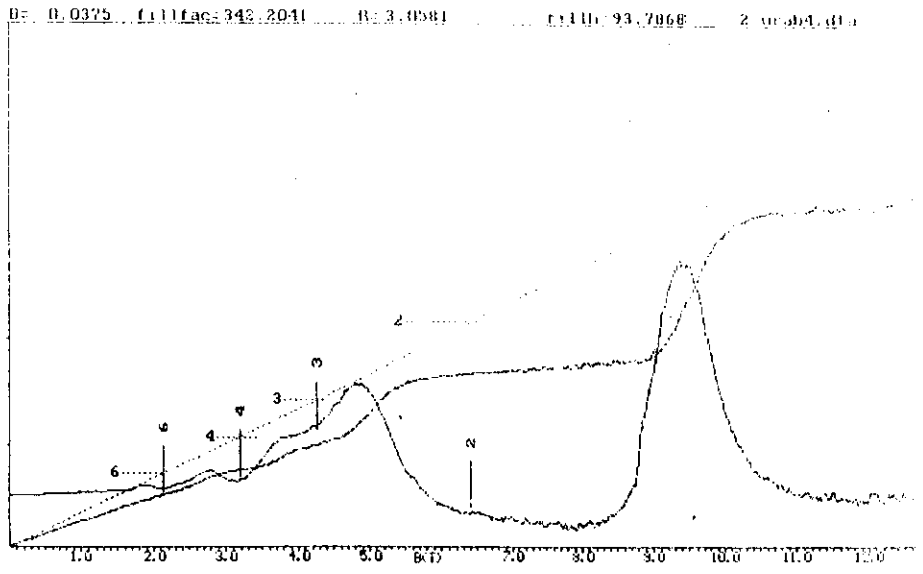

Fig. 30

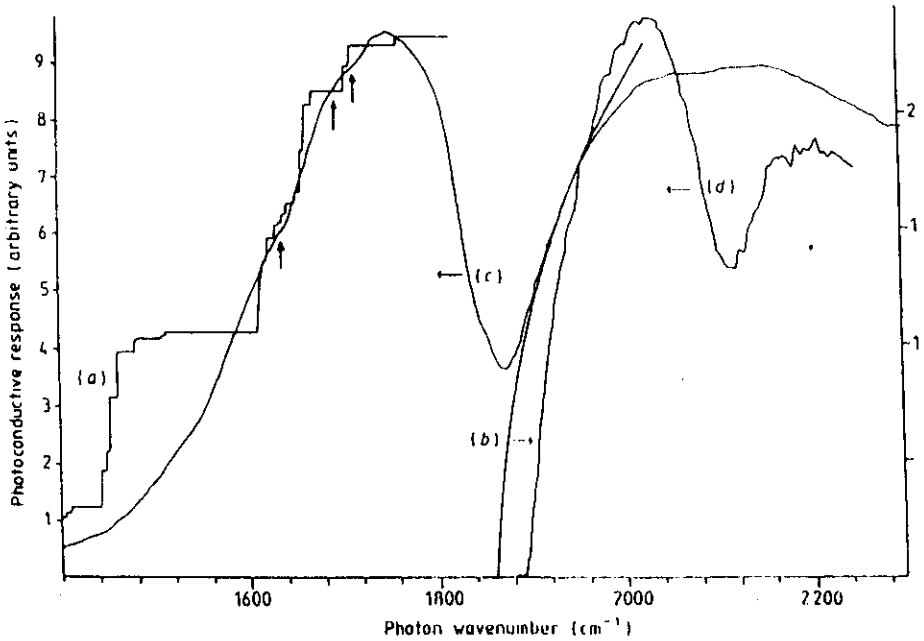

Fig 31

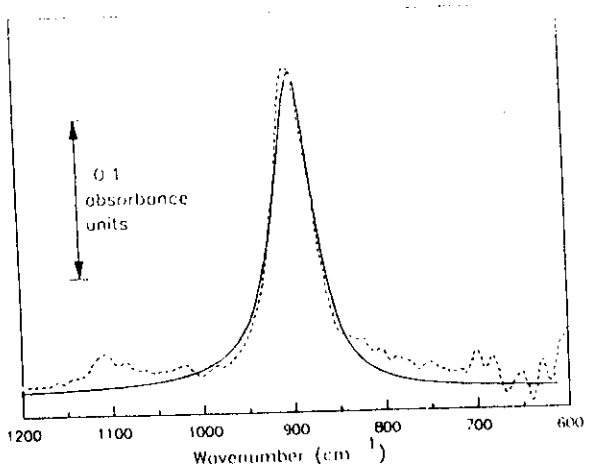

References

[1]. S.N. Holmes, R.A. Stradling, P.D. Wang, R. Droopad, S.D. Parker & R. L. Williams
Semicond. Sci & Tech. 4 303-308 (1989)

[2]. S.D. Parker, R. L. Williams, R. Droopad, R.A. Stradling, K.W.J. Barnham, S.N. Holmes, J. Laverty, C.C. Phillips, E. Skuras, R. Thomas, X. Zhang, A. Staton-Bevan & D.W. Pashley
Semicond. Sci & Tech. 4 663 (1989)

[3]. W.E. Spicer et al
J. Vac. Sci & Tech.16 1427 (1979)

[4]. W. Walukiewicz
J. Vac. Sci & Tech. B6 1257 (1988)
Phys. Rev. B37 4760 (1988)

[5]. W. Monch
Rep. on Progress in Physics 53 221 (1990).

[6] R. Droopad, R.L. Williams & S.D. Parker
Semicond. Sci & Tech. 4 111-113 (1989).

[7]. V.M. Glazov & E.B. Smirnova
Sov. Phys. Semicond. 17 1177 (1983).

[8] R.A. Kubiak, J.J. Harris & P. Dawson J. App. Phys. 55 598 (1984)

[9] R.M. Biefeld, S.R. Kurtz & I.J. Fritz
J. Electronic Materials 18 775 (1989)

[10] G.M. Williams, C.R. Whitehouse, T. Martin, N.G. Chew, A.G. Cullis, T. Ashley, D.E. Sykes, K. Mackey & R.H. Williams J. App. Phys. 63 1526 (1988)

[11]. S.R. Kurtz, G.C. Osbourn, R.M. Biefeld & S.R. Lee
Appl. Phys. Lett. 53 216 (1988).

[12]. T.Y. Seong, A.G. Norman, G.R. Booker, R. Droopad, S.D. Parker, R.L. Williams & R.A. Stradling
Materials Research Society Symposium Proceedings (1989)

[13] W. Dobbelaere, J. De Boeck & G. Borghs
App. Phys. Lett. 55 1856 (1989)

[14]. G. Hasnain, B.F. Levine, D.L. Sivco & A.Y. Cho
App. Phys. Lett. 56 770 (1990).

[15]. G. Tuttle, H. Kroemer & J.H. English
J. App. Phys. 65 5239 (1989).

[16]. G. Tuttle, H. Kroemer & J.H. English
J. App. Phys. (1990).

[17] A.J. Noreika, W.J. Takei, M.H. Francombe & C.E.C. Wood
J. App. Phys. 53 4932 (1982)

[18] K.Y. Ma, Z.M. Fang, D.H. Jaw, R.M. Cohen, G.B. Stringfellow, W.P. Kosar & D.W. Brown App. Phys. Lett. 55 2420 (1989).

[19]. X. Zhang, A.E. Staton-Bevan, D.W. Pashley, S.D. Parker, R. Droopad, R.L. Williams & R.C. Newman J.App Phys. 67 800 (1990).

[20]. T.S. Rao, C. Halpin, J.B. Webb, J.P. Noad & J. McCaffrey
J. App. Phys. 65 585 (1989) also J.B. Webb, M. Paiment & T.S. Rao
Solid State Comm. 71 871 (1989)

[21] W.T. Read
Phil. Mag. 45 111 (1954) & 46 111 (1955)

[22]. L.C.. Kimerling & J.R. Patel
VLSI Electronics Vol 12 223 (1985) (Ac. Press).

[23] H. Kroemer, T.Y. Liu & P.M. Petroff
J. Cryst. Growth 95 96 (1989)

[24]. G. Griffiths, K. Mohammed, S. Subbana, H. Kroemer & J.L. Merz
App. Phys. Lett. 43 1059 (1983).

[25]. J.Y. Marzin
Optical Properties of Narrow Gap Low-Dimensional Semiconductors
NATO ASI Series Vol B152 99 (1987).

[26] M. Sato & Y. Horikoshi
J. App. Phys. 66 851 (1989).

[27] G.C. Osbourn
J. Vac. Sci. & Tech. B2 176 (1984).

[28] J.R. Dawson
J.Cryst. Growth 98 220 (1989).

[29] S. Groves & W. Paul Phys. Rev. Lett. 11 194 (1963)

[30] B.L. Booth & A.W. Ewald Phys. Rev. 186 770 (1969).

[31] S. Groves Physics of Semimetals & Narrow Gap Semiconductors (ed D.L. Carter & R.T. Bate - Pergamon) p 447 (1971).

[32] B.L. Booth & A.W. Ewald Phys. Rev. Lett. 18 491 (1967)

[33] R.C. Farrow et al
J. Cryst. Growth 54 507 (1981).

[34] E.A. Fitzgerald,P.E. Freeland, M.T. Asom, W. Lowe, R. MacHarrie, A.R. Kortan, Y.H. Xie, F.A. Thiel,A.M. Sargent L. Cooper, G.A. Thomas, K.A. Jackson, B.E. Weir, G.P. Schwartz, G.J. Gualtieri & L.C. Kimmerling Abstracts 119th TMS Annual Meeting p31 (1990).

[35] S. Takatani & Y.W. Chung Phys. Rev. B31 2290 (1985)

[36] B.I. Craig & B.J. Garrison Phys. Rev. 33 8130 (1986)

[37] Li-Wei Tu, G.K. Wong & J.B. Ketterson App. Phys. Lett. 55 1327 (1989)

[38]. W.T. Yuen, W.K. Liu, B.A. Joyce & R.A. Stradling Semicond. Sci & Tech. 5 (1990)

[39]. W.T. Yuen, W.K. Liu, S.N. Holmes & R.A.Stradling Semicond. Sci & Tech 4 819 (1989)

[40] L. Liu Physics Lett. 45A 285 (1973) & Solid State Comm. 16 285 (1975)

[41] M.T. Asom, E.A. Fitzgerald, A.R. Kortan, B. Spear & L.C. Kimerling App. Phys. Lett. 55 578 (1989)

[42] P.R. Pukite, A. Harwit & S.S. Iyer App. Phys. Lett. 54 2142 (1989)

[43] A. Zrenner, F. Koch & K. Ploog Surface Science 196 671 (1988)

[44] M. Santos, T. Sajoto, A. Zrenner & M. Shayegan
App. Phys. Lett. 53 2504 (1988)

[45] A. Zrenner, F. Koch, R.L. Williams, R.A. Stradling, K. Ploog & G. Weimann Semicond. Sci. & Tech. 3 1203 (1988)

[46] E.F. Schubert, T.H. Chiu, J.E. Cunningham, B. Tell & E.F. Schubert
J. App. Phys. 64 1578 (1988)

[47] E.F. Schubert, J.B. Stark, B. Ulbrich & J.E. Cunningham
App. Phys. Lett. 52 1508 (1988)

[48] R.B. Beall, J.B. Clegg & J.J. Harris
Semicond. Sci & Tech. 3 612 (1988)

[49] A.M. Lanzillotto, M. Santos & M. Shayegan
App. Phys. Lett. 55 1445 (1989)

[50] N. Kobayashi, T. Makimoto & Y Horikoshi Jap. J. App. Phys. 25 L746 (1986)

[51] K. Ploog, M. Hauser & A. Fischer App. Phys. A 45 233 (1988)

[52] T. Ishikawa, K. Ogasawara, T. Nakamura & K. Kondo
J. App. Phys. 61 1937 (1987)

[53] E.F. Schubert, J.E. Cunningham, W.T. Tsang & G.L. Timp
App. Phy. Lett. 51 1170 (1987)

[54] H.P. Zeindl, T. Wegehaupt, I. Eisele, H. Oppolzer, H. Reisenger, G. Tempel & F. Koch App. Phys. Lett. 50 1164 (1987)

[55] M.W. Denhoff, T.E. Jackman, J.P. McCaffrey, J.A. Jackman, W.N. Lennard & G. Massoumi App. Phys. Lett. 54 1332 (1989)

[56] K. Nakagawa, A.A. van Gorkum & Y. Shiraki
App. Phys.Lett. 54 1869 (1989)

[57] H.M. Li, K.F. Berggren, W.X. Ni, B.E. Sernelius, M. Willander & G.V. Hansson J. App. Phys. 67 1962 (1990

[58] R.L. Williams, E. Skuras, R.A. Stradling, R. Droopad, S.N. Holmes & S.D. Parker.
Semicond. Sci & Tech. 5 (1990)

[59] E.A. Johnson & A. Mackinnon
Semicond. Sci. & Tech. 5 (1990).

[60] A. Mohades-Kassi, M.R. Brozel, R. Murray & R.C. Newman
GaAs & Related Compounds (1990)

[61] G.H. Dohler Phys. Stat. Solidi B52 79, 533 (1972)

[62] K. Ploog & G.H. Dohler Adv. Phs. 32 285 (1983)

[63] E.F. Schubert, T.D. Harris & J.E. Cunningham
App.Phys. Lett. 53 2208 (1988)

[64] B. Ullrich, C. Zhang & K. von Klitzing
App. Phys. Lett. 54 1133 (1989)
[65] E.F. Schubert, T.D. Harris , J.E. Cunningham & W. Jan
Phys. Rev. B 39 11011 (1989)

[66] E.F. Schubert, J.E. Cunningham & W.T. Tsang
App. Phys. Lett. 51 817 (1987)

[67] E.F. Schubert to be published

[68]. C.C. Phillips, C. Hodge, R. Thomas, S.D. Parker, R.L. Williams & R. Droopad Semicond. Sci. & Tech 5 (1990)

[69] C.C. Phillips App. Phys. Lett. 56 151 (1990).

[70] J. Maserjian, F.J. Grunthaner & C.T. Elliott
Infrared Physics 30 27 (1990)

[71] B.F. Levine, C.G. Bethea, G. Hasnain, J. Walker & R. J. Malik
App. Phys. Lett. 53 296 (1988)

[72] M.A. Kinch & A. Yariv App. Phys. Lett. 55 2093 (1989)

[73] C.T. Elliott, A. Davis & A.M. White
Semicond. Sci \ Tech. 5 (1990)

[74] K.W. Goossen, S.A. Lyon & K. Alavi
App. Phys. Lett. 53 1027 (1988)

[75] D.R.P. Guy, N. Apsley, L.L. Taylor, S.J. Bass & P.C. Klipstein
Quantum Well & Superlattice Physics (ed G.H. Dohler & J.N. Schulman - pub SPIE) (1987).

[76] J.Y. Andersson & G. Landgren J. App. Phys. 64 4123 (1988)

[77] B.C. Covington, C.C. Lee, B.H. Hu, H.F. Taylor & D.C. Streit
App. Phys. Lett 54 2145 (1989)

[78] F. Muller, V. Petrova-Koch, M. Zachau, F. Koch, D. Grutzmacher, R. Meyer, H. Jurgensen & P. Balk Semicond. Sci & Tech 3 797 (1988)

[79] M.J. Kane, L.L. Taylor, N. Apsley & S.J. Bass
Semicond. Sci & Tech. 3 586 (1988)

[80] F.H. Julien, J.M. Lourtioz, N. Herschkorn D. Delacourt, J.P. Pocholle, M. Papuchon, R. Planel & G. Le Roux
App. Phys. Lett. 53 116 (1988)

APPENDIX A THE USE OF FARINFRARED TECHNIQUES TO CHARACTERISE SEMICONDUCTORS

A1 CYCLOTRON RESONANCE IN BULK SEMICONDUCTORS

The treatment of the conductivity tensor outlined elsewhere can be generalised to include AC phenomena in a magnetic field. At frequencies (Ω) much higher than the plasma frequency ($\Omega_p^2 = ne^2/\epsilon\epsilon_o m^*$), depolarisation charges do not have time to become established and Hall fields are not present. It is helpful to resolve a linearly-polarised electric field applied in the x-direction into circularly-polarised components of the form

$$\tilde{E} = E_o(1 \pm j)\exp(j\Omega t) \qquad (A1)$$

Provided no depolarisation charge has built-up, the resultant circulating currents in the x-y plane can be written as

$$\tilde{J} = \tilde{\sigma}\tilde{E} \qquad (A2)$$

where a complex ac conductivity is given by

$$\tilde{\sigma} = \sigma_o/[1 + j(\Omega \pm \Omega_c)\tau], \quad \Omega_c = qB/m^* \qquad (A3)$$

where the $\pm$ symbol refers to the different senses of circular polarisation of the electromagnetic field.

The resultant power loss per unit volume arising from the circulating currents can be written as

$$P = \tilde{J}.\tilde{E} = \sigma_o E_o^2/[1 + (\Omega \pm \Omega_c)^2\tau^2] \qquad (A4)$$

If the carrier concentration is so low that the skin depth is much greater than the thickness of the sample, the electric field at all points in the sample is independent of the magnetic field and the total power absorbed as measured by the transmission of radiation from the sample or the power loss in an external resonant circuit is given by equation (A4). As can be seen from this equation, the absorption of power by the free carriers is sharply peaked when $\Omega = \Omega_c$ for the negative sign in the denominator which corresponds to the sense of circular polarisation circulating in the same sense as the carriers provided that $\Omega\tau >> 1$. This resonant absorption of power is known as cyclotron resonance and is the most direct and accurate method of measuring the effective mass of the charge carriers (from the resonant condition $\Omega = \Omega_c$) provided that the necessary experimental conditions can be established.

The collision time can be deduced directly from the width of the cyclotron resonance absorption from the relation $B/\Delta B = \Omega\tau$. An absolute value for the carrier concentration can be found from the peak absorption and the values for τ and m^* deduced from the width and position of the cyclotron resonance line.

The condition that $\Omega\tau > 1$, which represents the requirement that the width of the cyclotron resonance line be sufficiently narrow for the observation of distinct peak, is rather demanding as, even with the purest samples available of the common semiconductors (apart from Si and Ge), the values of τ are typically 10^{-11}s. The experiment thus requires submillimetre wavelengths for the sources of the electromagnetic radiation and the use of very high magnetic fields to attain the resonance condition. Low temperatures are also desirable in order to reduce phonon scattering.

A2. PLASMA EDGE MEASUREMENTS OF CARRIER CONCENTRATIONS AND OTHER HIGH-FREQUENCY EFFECTS IN BULK SAMPLES

If the carrier concentrations are high, depolarisation (or 'plasma') effects can become important. Even if depolarisation charges do not become established at the surface of the sample, the cyclotron motion can become coupled to the plasma oscillations and the maximum absorption corresponds to the peak response of the system as a whole. At the same time the skin depth is likely to become less than the sample thickness and dependent on the magnetic field. In this case, the 'equation of telegraphy' arising from Maxwell's equations

$$\nabla^2 E = \frac{\mu\epsilon}{c^2}\frac{\delta^2 E}{\delta t^2} + \mu\mu_o\sigma\frac{\delta E}{\delta t} \qquad (A5)$$

must be used to derive a complex refractive index (n) which includes the free carrier term

$$n^2 = \mu\epsilon - j(\sigma\mu/\Omega\epsilon_o) \qquad (A6)$$

If the carrier density is very high so that the first term in equation (A6) can be neglected and the frequency is much less than the scattering rate (i.e. $\Omega\tau << 1$), the classical skin effect is found and the radiation penetrates a depth (δ) into the sample given by (A7)

$$\delta^2 = 1/(\pi\sigma f\mu\mu_o) \qquad \text{where } f = \Omega/2\pi. \qquad (A7)$$

If alternatively the frequency is much greater than the scattering rate ($\Omega\tau >> 1$), the complex refractive index is given by (8)

$$n^2 \approx \epsilon[1 - \Omega_p^2/\Omega^2] \text{ where } \Omega_p^2 = ne^2/m^*\epsilon\epsilon_o \qquad (A8)$$

provided the material is not magnetic ($\mu = 1$). Equation (A8) predicts that the sample is completely reflecting at low frequencies because the refractive index is purely imaginary. When $\Omega > \Omega_p$, the refractive index is real and the radiation starts to penetrate into the sample. When n=1, the sample becomes matched to free space and the reflection drops to zero (see figure 1). The abrupt change in reflectivity from the sample being totally reflecting to having zero reflection is known as the 'plasma edge' in the plot of reflectivity against frequency. This phenomenon is responsible for the ease of transmission of

long-wavelength radiowaves which are reflected from the ionosphere. However, when the frequency of the radio waves is greater than the plasma frequency of the ionised gas in the ionosphere (~10MHz), near line-of-sight transmission must be used. With metals the plasma frequency is in the ultraviolet and consequently most metals appear silvery (ie totally reflecting) at visible wavelengths.

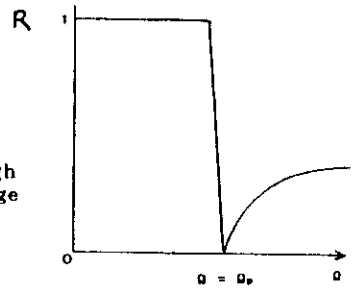

Figure A1 shows the reflectivity (R) against frequency (ω) for a highly conducting sample in the limit of high frequencies ($\omega\tau \gg 1$). The abrupt change from total reflection to transmission is known as the 'plasma edge'.

With semiconductors having carrier concentrations in the range 10^{14} to 10^{20} cm^{-3}, the plasma frequency occurs in the mid-infrared region of the spectrum and the assumption that $\omega\tau \gg 1$ applies. Consequently a well-defined 'plasma-edge' can be seen in the propagation constants and this can be used to provide an accurate and contactless method of determining the carrier concentration present in a sample provided that the effective mass is known. Such measurements can be used to determine the carrier concentrations and profiles in ion-implanted conducting skins in silicon extending only distances of the order of 5×10^{-5} cm^{-3} from the surface.

A3 INFRARED MEASUREMENTS OF THICKNESS OF THIN HETEROEPITAXIAL LAYERS

The techniques available to determine the thickness of epitaxial films include a careful calibration of the growth rate by means of the period of RHEED oscillations, TEM, Talystep measurements of the height of an etched region and infrared measurements of the Fabry-Perot interference fringes between the front and back surfaces of the film. Of the post-growth methods the latter is the most direct and one of the more accurate with the additional advantages of being rapid, non-destructive and requiring no substrate preparation. The infrared measurements can frequently be combined with a determination of the energy of the band edge. With doped samples the plasma edge can also be observed at long wavelengths. With doped samples also the position of the band edge will be shifted by the Moss-Burstein effect so that a scan of the optical properties from near to farinfrared wave lengths will not only give the sample thickness rather accurately but will also give two independent checks on the carrier concentration.

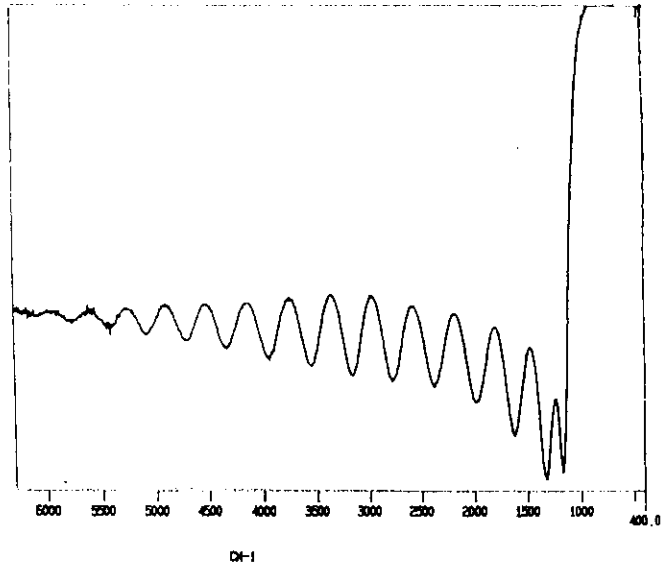

Figure A2 shows the plasma 'edge' and Fabry Perot interference fringes for a heavily doped hetero-epitaxial layer of InAs on GaAs (n ~5×10^{19} cm^{-3})

A4. INFRARED STUDIES OF ELECTRONIC ABSORPTION FROM IMPURITIES IN BULK SAMPLES

Bound states of substitutional impurities are described by a 'hydrogenic' model in elementary texts. A single electron (or hole) is assumed to be bound by a single fixed charge of opposite sign on the impurity, the Coulomb potential is modified to include the dielectric constant ϵ and the inertial mass of the free electron is replaced by the effective mass of the free carrier to include the interaction with the periodic crystal potential. The energy levels for the impurities are then given by the well-known hydrogenic formula

$$W^*_n = -13.6[m^*/m]/\epsilon^2 n^2 \quad \text{(eV)} \qquad \text{(A9)}$$

Typically m^*/m 0.1 and ϵ 10, so the ground state energy is reduced from the value for the hydrogen atom of -13.6 eV to about -10 meV. The wavelengths corresponding to typical binding energies lie in the range from the submillimetre to mid-infrared region of the spectrum. The Bohr radii of the bound states are very much extended in comparison with the hydrogen atom and are given by

$$a^*_n = 0.053 n^2 \epsilon/[m^*/m] \quad \text{(nm)} \qquad \text{(A10)}$$

This model provides an adequate first-order picture of the bound states of most shallow impurities. However, the theory breaks down to a greater or lesser extent for the following reasons:

i) Within the 'central cell' (ie the unit cell where the impurity is located), the potential is different from the $[-1/4\pi\epsilon\epsilon_0 r]$ form assumed in the hydrogenic model. As the 1s ground state wavefunction has its maximum amplitude at the origin, substantial shifts in energy can occur for this state. The resultant chemical shifts are characteristic of the impurity concerned. It should also be noted that both the effective mass approximation and the assumption of a macroscopic dielectric constant break down close to the central cell region. Corrections arising from the failure of these assumptions will however be the same for all impurities to first order.
ii) The assumption of a single effective mass cannot take into account such complexities as degenerate valence bands, the ellipsoidal constant energy surfaces and tensor effective masses that occur for the conduction bands of Si and Ge, band-nonparabolicity, or more complex dispersion relations such as the 'camel's back' shape that occurs in the conduction band of GaP.
iii) Self-energy phenomena such as the polaron effect that arises through interaction with the phonons.

As electric dipole transitions are involved, the absorption is relatively strong and concentrations of shallow impurities of $10^{11}cm^{-3}$ can be detected with sample thicknesses of 1mm. With thin films, even higher sensitivity can be achieved by detection of the photocurrent generated within the sample itself. The sharp bound-to-bound transitions can be observed through a two-stage 'photothermal' process where the carrier after photoexcitation into the higher bound state transfers into the conduction or valence band by the subsequent absorption of a phonon. By this means concentrations as low as 10^7cm^{-3} of minority impurities can be detected in ultrahigh purity germanium, and as few as 10^4 neutral phosphorus donors have been detected at the edge of the depletion region of a silicon MOSFET structure [Nicholas et al, 1976].

Because the chemical shifts are characteristic of the impurities, infrared spectroscopy can be used to characterise the residual contaminants present in material grown without deliberate doping. Very high resolution can be achieved in the far-infrared by the use of laser techniques. Figure A2(a) shows a recording of the photoconductivity obtained from the shallow donors by using a fixed frequency laser and sweeping the magnetic field applied to the shallow donors in an MOCVD sample of InP. This recording demonstrates the richness of the structure which can be observed. Up to fifty diiferent transitions can be observed. Fine structure can be seen on the 1s-2p lines (using low field nomenclature) arises from the presence of several contaminating donors in this sample. Figure A2(b) shows on an expanded scale the different donors present in a series of MOCVD and MOMBE samples of GaAs. [Armistead et al, 1989; Holmes et al, 1989b]. It should be noted that the difference in energy of the different donors is only 50 μeV i.e. approximately 1% of the binding energy of the effective mass binding energy (5.8 meV). Information about the nature of the contaminating shallow donors has been derived with comparable resolution with InP and InSb. In contrast, two activation energies cannot be distinguished in Hall measurements if they lie within a factor of two of each other.

APPENDIX B: MULTIPLE CARRIER EFFECTS

Even if the systematic errors that can arise from faulty measurement techniques or inhomogeneous samples are avoided, perfectly good experimental data can be misinterpreted through a failure to appreciate the assumptions implicit in the simple classical treatment of conduction in a magnetic field. The most basic of these is the assumption that all carriers have the same drift velocity. If this were correct, there would be no magnetoresistance whereas all semiconductors show a magnetoresistance to a greater or lesser extent.

The most common reason why a single carrier system with an isotropic effective mass shows a magnetoresistance is that the scattering is energy dependent. Appropriate averages have then to be taken for the collision times over the range of carrier energies. The Hall coefficient R is no longer independent of magnetic field but decreases from r/nq in the limit of low magnetic fields ($\mu B \ll 1$) to 1/nq at high fields ($\mu B \gg 1$) where n is the carrier concentration and q = ±e depending on carrier type. The Hall factor or constant (r) is given by

$$r = \langle\tau^2\rangle/\langle\tau\rangle^2 \qquad (B1)$$

In the case of ionised impurity scattering, using a simple Rutherford model, the numerical value for r is found to be $315\pi/512$. Consequently, although carrier concentrations deduced from the simplistic use of R = 1/nq in the low field regime are frequently quoted to three places, it should be realised that the systematic error could approach 100% if ionised impurity scattering is limiting the mobility unless correction is made for r. Smaller but still very substantial errors are present with other scattering mechanisms if classical statistics apply to the carrier distribution.

If two or more distinct carrier species are present, then both the magnetoresistance and the difference between the low and high field Hall coefficients become larger. Multiple carrier groups can occur because of the presence of light and heavy holes, electrons and holes in semimetals or near intrinsic semiconductors or because of degenerate conduction band minima such as occur with silicon and germanium. Parallel conduction in a layered system is also an example of conduction involving multiple carrier types although the carriers do not occupy the same space. The case of electrons in silicon and germanium must be treated with particular care as the tensor effective masses concerned imply that the drift velocity may not always be colinear with the accelerating force. Unless the magnetic field is applied along a direction where all the constant energy ellipsoids are equivalently oriented, several groups of carriers, all with

different masses, will result.

The Hall coefficient for a two carrier system is given by

$$R = \frac{\pm n_1\mu_1^2 \pm n_2\mu_2^2}{e(n_1\mu_1 + n_2\mu_2)^2} \qquad \text{at low fields} \qquad (B2)$$

or by $$R = \frac{1}{e(\pm n_1 \pm n_2)} \qquad \text{at high fields} \qquad (B3)$$

The low-field mobility, as measured in a Hall experiment and defined as Ro, is then given by

$$\mu_H = \frac{|\pm n_1\mu_1^2 \pm n_2\mu_2^2|}{(n_1\mu_1 + n_2\mu_2)} = R\sigma \qquad (B4)$$

where q = ±e and the positive and negative signs refer to hole and electron transport respectively. Equation (B3) is derived by writing $\sigma_{xy} >> \sigma_{xx}$. However, in the intrinsic case where the electron (n) and hole (p) concentrations are equal, $\sigma_{xy} \to 0$ and equation (B3), which predicts an infinite Hall voltage when n=p, is not correct. Instead R > 0 at high fields for intrinsic conduction.

The variation with temperature of the Hall coefficient can be used to measure the energy gap or the impurity activation energy involved whereas the Hall mobility (Rσ) is generally used to determine the nature of the scattering mechanisms concerned. With a single carrier it would appear to be preferable to use the high magnetic field limit as it may not be possible to estimate the Hall factor r accurately, particularly when the averaging over the carrier distribution is complicated by the presence of two scattering process with different energy dependencies. However, in most cases, the magnetic fields required to reach the high field limit are unavailable. Even if it is possible to satisfy the condition μB >> 1, the onset of various quantum limit phenomena such as the Shubnikov-de Haas effect or magnetic freeze-out may complicate the interpretation still further. Consequently systematic errors can creep into the measurement of both energy or mobility.

When two or more carriers are present, the analysis is even more complicated as the individual carrier concentrations and mobilities must be estimated if activation energies are to be derived at all accurately.

Despite these difficulties, Hall effect and conductivity measurements are used widely and successfully to determine the electrical properties of semiconductor samples including carrier concentrations, mobility, band gap and impurity activation energies, density-of-states for the bands concerned and to determine the scattering processes concerned (see general reviews by Putley, 1960; Wieder 1979).

APPENDIX C. QUANTUM TRANSPORT EFFECTS

The simple Drude-Sommerfeld approach used so far in this article, and other classical treatments such as the Boltzmann equation, break down in the quantum limit when the separation between the Landau levels becomes greater than the thermal energy ($\hbar\Omega_c > k_BT$). Under these conditions, a number of new phenomena become apparent in the electrical resistance of semiconductors. Of these the most studied is the Shubnikov-de Haas effect which is discussed in sections four and five of the mainarticle.

C.1 THE SHUBNIKOV-DE HAAS EFFECT

The Shubnikov-de Haas effect represents an oscillatory variation of the electrical resistance which is periodic in reciprocal magnetic field. The scattering-rate peaks when each Landau level empties. In order that this variation be observable, the carrier distribution must be degenerate (ie the Fermi energy $E_F >> k_BT$), the sample must be of high purity and the magnetic field must be high ($\hbar\Omega_c >> k_BT$ and $\Omega_c\tau >> 1$). Under these conditions the resistance in a magnetic field should be described by the following expressions [see Roth & Argyres, 1966, Kubo et al, 1965]. The scattering rate and hence the resistance show peaks at values of magnetic field close to the fields where the Landau levels empty. This result arises from the form of the one-dimensional density-of-states function which varies as $E^{-\frac{1}{2}}$ where E is the kinetic energy along the magnetic field. Provided that the peaks are not too sharp, the resistance is given by

$$\sigma_{zz}/\sigma_0 = 1 + b\cos(2\pi F/B - \pi/4) \qquad (C1)$$

$$\sigma_{xx}/\sigma_0 = 1 + 2.5\, b\cos(2\pi F/B - \pi/4) + R \qquad (C2)$$

where $$b = -\left(\frac{\hbar\Omega_c}{2E_F}\right)^{\frac{1}{2}} \frac{\cos(\pi\nu)\, X \exp(-2\pi/\Omega_c\tau)}{\sinh X} \qquad (C3)$$

and

$$X = 2\pi^2 k_BT/\hbar\Omega_c \qquad F = E_Fm^*/\hbar e \qquad \nu = g^*m^*/2m \qquad (C4)$$

In the equations above, E_F is the Fermi energy and g^* is the effective Landé g-value for the carriers. The cosine terms in equations (C1) and (C2) determine the period in inverse magnetic field (1/B) of the resistance oscillations.

For a single isotropic band,

$$F = \hbar k_F^2/2e = \hbar(3\pi^2 n)^{2/3}/2e \qquad (C5)$$

where k_F is the wavevector of the carriers at the Fermi surface.

Thus $$n = (s/6\pi^2)\,(2e/\hbar)^{3/2}\,[\delta(1/B)]^{-1} \qquad (C6)$$

where s represents the spin-degeneracy (ie. s = 2 in equation (C6) if spin-splitting is not resolved).

Thus the number of carriers can be obtained directly from the period of the oscillations by means of equation C6 without the uncertainty associated with the estimation of the Hall factor (r). With an anisotropic Fermi surface, the dependence of the period on the orientation of the magnetic field with respect to the crystal axes gives the anisotropy of the extremal cross-sectional areas ($F = \hbar A/2\pi e$). Note that measurements of the size or shape of the Fermi surface are completely independent of the effective mass of the charge carriers. Equations (C1) and (C2) are in effect the first terms of Fourier expansions describing the periodic variation of the scattering rate as each Landau level empties with increasing magnetic field. The b term contains the temperature dependence of the oscillations through the factor X/sinhX which for large values of X is dominated by the term exp-X. The effective mass of the charge carriers can be determined from fitting the temperature dependence of the amplitude to this expression. Note that the Shubnikov-de Haas oscillations reach their maximum amplitude only when X/sinh X -> 1 or when $\hbar\Omega_c \geq 20k_BT$ which provides a demanding requirement on the experimental low temperature/high field facilities.

The R term in equation (C2) represents a phase shift of the oscillations arising from the competition between inter and intra Landau level scattering processes. This phase factor changes as a function of field. The exp ($-2\pi/\mu B$) term in equation (C3) arises from the broadening of the Landau levels by scattering. By fitting the magnetic field dependence of the oscillations to this expression the mobility can be measured. The cos ($\pi\nu$) term is generated by the spin-splitting of the Landau levels. If $\Omega_c\tau \gg 1$, higher order Fourier terms must be included in eqtns. (C1) to (C3) and spin-splitting of the Landau levels becomes apparent enabling the effective g-value for the carriers to be determined directly.

Hence all the main parameters for the free carriers can be measured directly from the Shubnikov-de Haas effect; i.e. the carrier density and the anisotropy of the bands from the positions of the peaks, the effective mass and the mobility of the carriers from the temperature and field-dependence of the amplitudes, and the effective g-value from the spin-splitting of the peaks.

The above analysis refers specifically to a normal bulk sample. However much of the treatment can be taken over for quasi-two dimensional samples which exhibit the Quantum Hall Effect in addition to Shubnikov-de Haas oscillations in the magneto-resistance. The carrier energy becomes completely quantised and, as a result, the density-of-states function for a two dimensional system lacks the $E^{-\frac{1}{2}}$ dependence on energy along the field. Equation C6 from which the electron concentration can be deduced for a bulk sample is modified in the case of a 2DEG to become

$$n = (es/h)\,[\delta(1/B)]^{-1} \qquad (C7)$$

In equation C7 s represents spin-degeneracy and should be taken as 2 if spin-splitting is not resolved but 1 if separate series due to spin-up and spin-down down oriented electrons are observed.

In the case of more than multiple subband occupancy, each subband will give rise to a separate series with its own periodicity and equation C7 will give the population of each occupied subband. In more than one series is present Fourier techniques may have to be used to determine the fundamental fields of the different series (the case of alpha tin/InSb structures discussed in section five provides an example of this situation).

Because the degree of translational freedom along the magnetic field is absent for a two-dimensional system, the amplitude of the resistance changes can become extremely great at high fields. Generally the magnitude of the higher order harmonics can therefore become quite large under these conditions (see figure C1). In the absence of any scattering the density-of-states simply consists of a series of delta-functions at the Landau level energies. If short-range point scatterers are responsible for broadening the Landau levels, a simple elliptic density-of-states function results. Any more complicated scattering process gives rise to exponentially-decaying tails in the density-of-states function with the states becoming more progressively localised with increasing energy difference from the centre of the Landau level. The treatment of quantum transport under these conditions involves considerable subtlety and caution must be applied in taking over ideas acquired from three dimensional quantum transport, particularly in cases where spin-splitting is important. The lack of the degree of translational freedom along the magnetic field and the associated piling-up of electronic states close to the unbroadened Landau level energies means that very considerable spin polarisation can be achieved when the Fermi energy is located near to the lowest Landau levels. As a result considerable enhancement of the electronic g-values will occur when the polarisation is large.

A further complication is that, even without significant enhancement of the electronic g-value, the separation in magnetic field of the spin-split peaks does not depend simply on the electronic g-value. If the spin-up and spin-down states do overlap at all at high fields, the Fermi level will jump discontinuously from one to the other as the magnetic field (or carrier concentration in a gated structure) is swept. Under these conditions a separate series of Shubnikov-de Haas resistance peaks will be observed for each spin-orientation. The two series will have a phase difference of π and each series will have double the fundamental field predicted from the low field oscillations (corresponding to s=1 in equation C7) . However, the effective mass and the mobility of the charge carriers can be found from

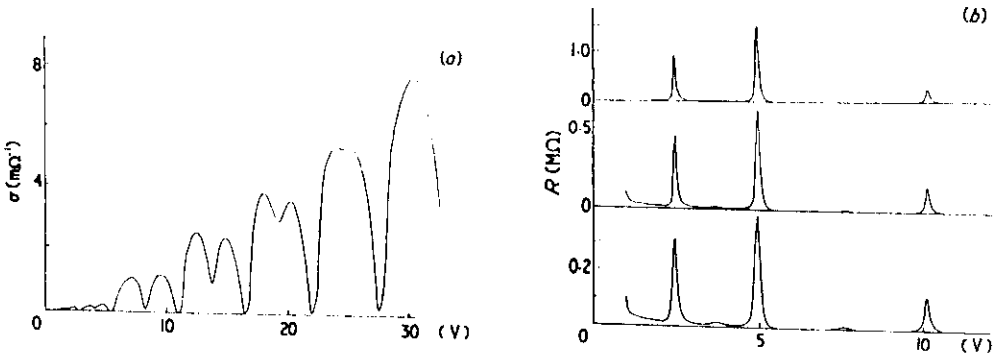

Figure C1 Experimental recordings of Shubnikov–de Haas effect in the inversion layer of a MOST. (*a*) shows the conductivity as a function of gate voltage for a magnetic field of 8·6 T. To illustrate the small value of the conductivity at the minima (*b*) shows a recording of the resistivity of the channel as a function of gate voltage for the first two Landau levels. The peaks in this recording correspond to the minima in (*a*). The different curves are plotted using a range of measuring currents and it is only at the lowest current that little damping of the peaks due to electron heating takes place.

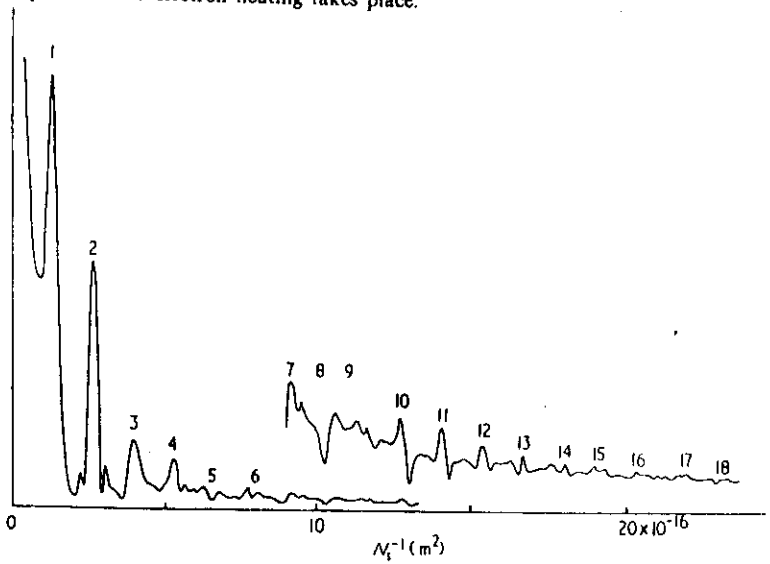

Figure C1 A Fourier transform of the conductivity of an MOST in a magnetic field with gate voltage as the transformed variable. The first peak corresponds to the fundamental periodicity in the density of states, ie the Landau level spacing. Up to the 18th harmonic of this fundamental are observed.

the temperature and field-dependence of the low-field oscillations in the same way as for a bulk sample.

All the discussion so far has implicitly assumed that the magnetic field is aligned perpendicular to the plane of the two dimensional electron gas. On tilting the magnetic field, the cyclotron orbits will be constrained to remain in the plane of 2DEG and consequently the Landau level separation will be determined by the component of field $B\cos\theta$ where θ is the tilt angle. As a result the Shubnikov de Haas peaks will characteristically move upwards in field as $1/\cos\theta$. However the spin energies depend only on the total value of the field and therefore will be unaffected by tilting the field. Consequently spin effects will become more pronounced as the ratio of spin-splitting to Landau splitting increases as $1/\cos\theta$.

This increase in magnitude of the spin-splitting with respect to the Landau energy can be utilised to determine the value of the electronic g-value from the amplitude of the weak-field Shubnikov-de Haas peaks. Under weak-field conditions only the first harmonic term is of significance in the Fourier series describing the amplitude of the oscillations. Each spin-orientation will give rise to a cosine series periodic in 1/B and exponentially damped in field. However the sum of two cosine series of equal amplitude is simply another cosine series whose amplitude is determined by the phase difference between the two series as described by equations C2 to C4. When the ratio of the spin-splitting to the Landau level energy is one half, the phase difference between the two series is π and the total amplitude therefore goes to zero. The value of θ at which the amplitude of the Shubnikov-de Haas peaks goes to zero gives the electronic g-value precisely provided that the effective mass is known. On increasing θ further the phase of the low field oscillations changes by π.

A value for g can also be deduced from field and angle at which spin-splitting of the high field peaks becomes first resolved according to the Rayleigh criterion provided that the width (Γ) of the Landau levels is known at the field concerned. The width Γ can be determined from the cyclotron resonance line width at the same field.

When the magnetic field is applied parallel to the plane of the 2DEG, Landau levels will not be formed (unless the diameter of the cyclotron orbits becomes less than the width of the confining potential). However the subbands will shift in energy by an amount given by

$$E = (e^2/2m^*)\{< z_i^2 > - < z_i >^2\} B^2 \qquad (C8)$$

Here $< >$ is the appropriate average of the extent of the electronic wavefunction in the z-th direction for the i^{th} subband. As the term $\{\ \}$ changes from subband to subband, an increasing magnetic field causes the higher subbands in turn to rise above the Fermi energy. Each subband redistributes its

carriers among the lower lying states. As each subband empties the resistance passes through a peak because of the enhanced scattering rate. This effect is called the 'diamagnetic' Shubnikov-de Haas effect and it causes a series of rather widely-spaced peaks which are not periodic in 1/B. Spin-splitting can also be seen on these peaks.

At tilted magnetic fields the diamagnetic depopulation of the subbands will cause the population of the lower subbands to increase and consequently there will be changes in periodicity of the different Shubnikov-de Haas series which may cause difficulties in interpretation.

Reisinger & Koch (1986) have analysed the diamagnetic Shubnikov-de Haas effect observed with parallel magnetic fields for the cases of the asymmetric potential for interfacial accumulation layers and for the symmetric potential found with spike or delta doped layer. Taking the peak value for dσ/dB (or dσ/dn) as corresponding to the depopulation of the particular subband concerned, they were able to generate universal curves applicable for all materials by plotting the field and total population in a dimensionless manner as $\gamma^* = \hbar\omega_c/R^*$ and $\bar{N}_s = N_s a^{*2}$ where ω_c is the cyclotron frequency, R^* is the effective Rydberg and a^* is the effective Bohr radius.

The condition for the depopulation of the i^{th} subband is then

$$\gamma^* = \alpha_i N_s \qquad \text{(C9)}$$

giving $$B_i = \alpha_i N_s (R_y a_o^2) m/\hbar e \qquad \text{(C10)}$$

Hence $$B_i = \alpha_i N_s (\hbar/2e) \qquad \text{(C11)}$$

$$= \alpha_i \times 3.28\times10^{-16} N_s \text{ with } N_s \text{ in } (m^{-2})$$

The values for α depend on the total occupancy N_s but only weakly and typical values at $\gamma^* \sim 10$ are given in the table below (on the assumption that spin-splitting is not resolved):

	Symmetric	Antisymmetric
α_1	2.7	2.7
α_2	0.92	0.85
α_3	0.35	0.25
α_4	0.05	0.15

The depopulation fields B_i may be related to the fundamental fields ($B_i^{\perp}$) for the Shubnikov-de Haas series observed with the field perpendicular to the plane of the 2DEG by combining equations C7 & C 11 to give:

$$B_i = \alpha_i (1/\pi) \Sigma_i B_i^{\perp} \quad \text{(taking s = 2)} \qquad \text{(C12)}$$

C.2 MAGNETIC FREEZE OUT

A further quantum effect, which can cause a large magneto-resistance in the high field limit is the decrease in free carrier concentration which will occur as a consequence of the decrease in extent of the impurity wavefunctions and increase in binding energy with increasing magnetic field ("magnetic freeze-out"). The effect is very much accentuated if the shrinkage of the size of the impurities induces the "metal-insulator" phase transition. The carriers which give rise to the Shubnikov-de Haas effect normally originate from impurities at concentrations which are above the critical concentration for the metal-insulator transition where the binding energy to the impurities goes to zero. It is therefore far from obvious that freeze-out will necessarily occur at higher fields than the low index (N≈1) Shubnikov-de Haas peaks. The following analysis shows that the magnetic-field induced metal-insulator phase transition and magnetic freeze-out occur close to but at slightly higher magnetic field than the N =1 peak. If spin-splitting is not observed, the N =1 Shubnikov-de Haas peak occurs at a field given by

$$B_{SH} \approx \frac{h(3\pi^2 n)^{2/3}}{3e} \quad \alpha \quad n^{2/3} \qquad \text{(C9)}$$

The Mott-Hubbard theory of the metal-insulator transition predicts that [Mott,1974]

$$n^{1/3} a^* \approx \tfrac{1}{4} \qquad \text{(C10)}$$

where a* is the effective Bohr radius for the impurities. In a magnetic field the impurity shrinks in size and becomes ellipsoidal in shape. In the high field limit, the extent of the impurity wavefunctions perpendicular to the magnetic field approximates to the cyclotron radius (r) in the quantum limit which is given by

$$r^2 = h/eB \qquad \text{(C11)}$$

At first sight, the extent of the impurity along the magnetic field should be given by the effective Bohr radius a*. In this case, the critical magnetic field B_c may be found by substituting the mean radius of the impurity $(r^2 a^*)^{1/3}$ into equation C10 to give

$$B_c \quad \alpha \quad n \qquad \text{(C12)}$$

On comparing equation C9 and C12 it is clear that there is an increasing difference between the critical field and the fields where the Shubnikov-de Haas effect is observed as n increases . However the assumption that the size of the impurity along the magnetic field is independent of field is incorrect. Yafet, Keyes and Adams (1956) showed that the extent of the impurity wavefunction along the field shrinks 'in sympathy' and the two fields diverge more slowly. As is shown below, the ratio of the two fields is independent of carrier concentration in the two dimensional case. For a 2DEG, the equivalent equation to C9 for

the position of the N=1 Shubnikov-de Haas peak is:

$$B_{SH} \approx \hbar n/3e \quad a \quad n \qquad \text{C13}$$

The condition for magnetic freeze-out can be written as

$$n^{\frac{1}{3}}r \approx \tfrac{1}{4} \qquad \text{C14}$$

giving

$$B_c \approx 16\hbar n/2\pi e \qquad \text{C15}$$

Comparing C12 and C15 it is seen that magnetic freeze-out for a 2DEG occurs close to but at rather higher fields than the lower order Shubnikov-de Haas peaks.

APPENDIX. REFERENCES

Argyres, P.M. & Adams E.M. (1956) Phys. Rev. **104** 900.

Armistead C.J., Stradling R.A. & Wasilewski Z. (1989) Semicon. Sci. & Tech.

Askenazy, S., (1973) New Developments in Semiconductors p331 Ed. P.R. Wallace, pub: Noordhoff.

Beer, A.C. (1963) Supp. No. 4 to Solid State Phys. (Ed. Seitz & Turnbull)

Eaves,L., Hoult, R.A., Stradling, R.A., Tidey, R.J., Portal, J.C. & Askenazy,S., (1975) J.Phys. C **8** 1034.

Holmes, S.N. et al (1989) Semicon. Sci. & Tech.**4** 303.

Kubo R., Miyake S. & Hashitsume N. (1965) Solid State Physics **17** 269 (Ed. Seitz & Turnbull).

Mott, N.F. (1974) Metal-Insulator Transitions (pub. by Taylor & Francis).

Nicholas, R.J., Von Klitzing K. & Stradling R.A., (1976) Solid State Comm. **20** 77.

Putley E.H. ,1960) The Hall Effect & Related Phenomena (Butterworth).

Reisinger H. & Koch F. (1986) Surface Science **170** 397

Roth L. & Argyres P.M. (1966) Semiconductors & Semimetals **1** 159.

van der Pauw L. Philips Research Reports (1958) **13** 1 & (1961) **20** 220

Wieder H.H. (1979) Laboratory Notes on Electrical and Galvanomagnetic Measurements (pub. Elsevier).

Weiss, H, (1967) Vol **1** Semiconductors & Semimetals & (1965) Solid State Electronics **8** 241

Yafet Y., Keyes R.W. & Adams E.N. (1956) J. Phys. Chem. Solids **1** 137